Challenges and strategies in the encapsulation and stabilization of monodisperse Au clusters within zeolites

CrossMark

Trenton Otto [a], Stacey I. Zones [b], Enrique Iglesia [a,c,*]

[a] Department of Chemical and Biomolecular Engineering, University of California at Berkeley, Berkeley, CA 94720, USA
[b] Chevron Energy Technology Company, Richmond, CA 94804, USA
[c] Division of Chemical Sciences, E.O. Lawrence Berkeley National Laboratory, Berkeley, CA 94720, USA

A B S T R A C T

This study describes successful strategies and guiding principles for the synthesis of small and monodisperse Au clusters protected against coalescence and poisoning by their uniform dispersion throughout the void space of LTA and MFI zeolites. These protocols involve hydrothermal zeolite crystallization around Au^{3+} precursors stabilized by mercaptosilane ligands, which prevent their premature reduction and enforce connectivity with incipient crystalline frameworks. The confining nanometer scale voids restrict cluster mobility during thermal treatment and allow the selection of reactants, products, and transition states and the exclusion of organosulfur poisons in catalytic applications based on molecular size. UV–visible spectra show that Au^{3+} forms Au^0 clusters in O_2 or H_2 in a narrow temperature range that sets the dynamics of nucleation and growth and thus cluster size. Reduction protocols that maintain stable temperatures at the lower end of this range lead to small clusters uniform in size (LTA: 1.3 nm, MFI: 2.0 nm; 1.06–1.09 dispersity indices) with clean and accessible surfaces, as shown by their infrared spectra upon chemisorption of CO. Their unprecedented size and monodispersity are retained during oxidative treatments (773–823 K) that sinter Au clusters on mesoporous supports. Oxidative dehydrogenation rates of small (ethanol) and large (isobutanol) alkanols and the poisoning of unprotected clusters by organosulfur titrants show that >90% of the Au surfaces reside within intracrystalline LTA and MFI voids. Their very different structures, compositions, and synthesis protocols suggest that these encapsulation strategies can be adapted readily to other zeolite frameworks with apertures too small for postsynthesis exchange of Au precursors. This study illustrates how confinement favors small, uniquely stable, and monodisperse clusters, even for Au, a metal prone to cluster growth at conditions often required for its catalytic use.

© 2016 Published by Elsevier Inc.

1. Introduction

The synthesis and the mechanistic interpretation of the reactivity of Au nanoparticles have attracted significant attention because of their unique catalytic properties and adsorbate binding characteristics, which resemble those of less noble Pt group metals in reactions as diverse as alkene epoxidation, CO oxidation, hydrogenation, and alcohol oxidation [1–3]. Preserving their monodisperse and small sizes (<5 nm) during thermal treatments and catalysis remains essential, because their unique properties are often conferred by coordinatively unsaturated surface atoms that prevail in small clusters [4,5]. These requirements present formidable challenges because of the low Tammann temperature of Au

(620 K) [6] and also because cluster melting points decrease markedly with decreasing particle size [7].

The encapsulation of nanoparticles within microporous solids may improve the inherent instability of Au nanoclusters by sequestering them within voids that prevent their coalescence with other clusters, while also restricting the size to which they can grow through spatial constraints. Confinement within such voids can also preclude access by reactants or poisons to Au surfaces, retain undesired products until they can convert and then diffuse as smaller species, or stabilize specific transition states, in all cases dictated by the size of the voids or channels in a specific microporous framework [8,9]. Strategies to confine Au within zeolites, however, often face synthetic challenges that prevent selective and efficient encapsulation.

Encapsulation within large-pore zeolites (12-member ring (12-MR) or larger) is relatively straightforward, because solvated metal cations can enter via exchange, impregnation, or adsorption

methods after the framework has formed [10]. Au clusters within such zeolites, however, often do not show greater stability than those prepared by colloidal precipitation methods and subsequent dispersion of clusters onto mesoporous scaffolds. For example, Au nanoparticles with ~3 nm mean diameter are present in FAU after exchange with Au(III)-ethylenediamine, but treatment in O_2 or H_2 at 473 K causes their growth to ~10 nm clusters [11]. Similar strategies in LTL zeolites initially form ~2 nm clusters that coalesce and grow to ~5 nm after treatment in air at 498 K [12]. The sputtering of Au metal onto SiO_2, in contrast, forms clusters with 3.2 nm mean diameter after treatment in O_2 at 773 K [6], while deposition-precipitation methods on γ-Al_2O_3 lead to 4 nm Au clusters after treatment at 873 K in O_2 [13]. Au can be simply encapsulated into large-pore zeolites, but these previous studies show that the clusters in these zeolites are often less stable than those on mesoporous scaffolds, in spite of the posited benefits of encapsulation.

Medium-pore (10-MR) zeolites with more constrained apertures, such as MFI, confer greater stability than large-pore materials, but reported synthetic procedures typically lead to bimodal size distributions, with a significant fraction of the clusters (>10 nm in size) at external MFI crystal surfaces [14,15]. The introduction of ligand-stabilized colloidal Au into an MFI synthesis gel led to the intact encapsulation of only a subset of these particles; the encapsulated clusters are stable at 823 K in air, but those excluded from the intracrystalline voids sinter to very large Au crystals (>20 nm) [15]. The impregnation of aqueous cationic Pt or Au precursors onto alkali-treated MFI (to form mesopores that enhance imbibition by these solutions) gave metal clusters with ~3 nm mean diameter after O_2 (823 K) or H_2 (623 K) treatments [5,16], but the significant fraction of the clusters present at external zeolite surfaces again formed large (>10 nm) clusters [16]. These diverse techniques have led to improved encapsulation and greater size stability of Au clusters, but they do not form encapsulated clusters of unimodal size or allow extensions to zeolites with even smaller apertures, for which impregnation or exchange is impossible because solvated precursors are much larger than the intracrystalline passages [8].

Here, we report the selective encapsulation of Au clusters into LTA (small-pore) and MFI (medium-pore) zeolites by incorporating ligand-stabilized monomeric Au^{3+} precursors into hydrothermal synthesis gels and decomposing such precursors after zeolite crystallization using protocols that lead to small and nearly monodisperse clusters (1–2 nm) with clean surfaces; these clusters remain stable against growth at 773 K in both H_2 and O_2 environments. Transmission electron microscopy (TEM), X-ray diffraction (XRD), and infrared (IR) spectroscopy of chemisorbed CO are used to determine the size and dispersity of Au clusters, the zeolite crystallinity, and the Au surface cleanliness, respectively. The bifunctional 3-mercaptopropyl-trimethoxysilane ligands provide chemical protection from reduction or precipitation of Au^{3+} precursors in strongly alkaline synthesis gels, while also promoting the nucleation of silicate oligomers around ligated metal precursors. The thiol group binds to Au^{3+} cations to form stable Au–S adducts [17,18] and the alkoxysilane moiety forms siloxane bridges with the silica precursors in alkaline conditions [19], thus encouraging the uniform dispersion of Au precursors throughout the zeolite crystals formed. Treatment in O_2 and then H_2 leads to 1–2 nm particles that are narrowly distributed in size (as determined by their dispersity index [8,9] (DI) values) and expose surfaces free of synthetic debris. Their mean diameter can be systematically varied without loss in monodispersity by varying the temperature of the post-synthetic H_2 treatment, which is shown by UV–vis spectroscopy to represent the most consequential synthesis stage for the formation of Au^0 and its nucleation and growth into clusters. These reduced clusters, once formed, do not coalesce during later

treatments in O_2 or H_2 environments up to 773 K, consistent with their encapsulation and protection by the intervening windows and cages within zeolite crystals.

The oxidative dehydrogenation (ODH) of large and small alkanols confirmed the extent and consequences of confinement. Ethanol (0.40 nm kinetic diameter) [9] ODH turnover rates are much higher than for isobutanol (0.55 nm) [9] on Au/CaLTA (0.50 nm apertures) [20], consistent with the exclusion of isobutanol from Au clusters within intracrystalline regions. Ethanol ODH rates after exposing AuNaLTA (0.42 nm apertures) [20] to thiophene (0.46 nm) [9] and AuNaMFI (0.55 nm apertures) [21] to dibenzothiophene (DBT, 0.9 nm kinetic diameter) [22] confirmed that active Au surfaces are protected from large titrants and predominantly confined within LTA and MFI voids.

2. Methods

2.1. Reagents

Ludox AS-30 colloidal silica (30 wt.% suspension in H_2O, Sigma–Aldrich), tetraethyl orthosilicate (TEOS; 98%, Sigma–Aldrich), fumed SiO_2 (Cab-O-Sil, HS-5, 310 $m^2\ g^{-1}$), 3-mercaptopropyl-trimethoxysilane (95%, Sigma–Aldrich), $NaAlO_2$ (53% Al_2O_3, 42.5% Na_2O, Riedel-de Haën), NaOH (99.99%, Sigma–Aldrich), 1 M tetrapropylammonium hydroxide (TPAOH; 98%, Sigma–Aldrich), $HAuCl_4$·$3H_2O$ (99.999%, Sigma–Aldrich), calcium chloride dihydrate (EMD Millipore), ethanol (99.9%, Sigma–Aldrich), isobutanol (99.9%, Sigma–Aldrich), thiophene (99%, Alfa Aesar), dibenzothiophene (98%, Sigma–Aldrich), ethylenediamine (98%, Sigma–Aldrich), acetone (99.9%, Sigma–Aldrich), He (99.999%, Praxair), 25% O_2/He (99.999%, Praxair), air (extra dry; 99.999%, Praxair), H_2 (99.999%, Praxair), and 1.0% CO/He (99.999%, Praxair) were used as received.

2.2. Synthesis of Au cluster catalysts in LTA, MFI, and mesoporous SiO_2

2.2.1. Au cluster encapsulation within LTA

Au-encapsulated Na-LTA zeolite (AuNaLTA) was prepared by adding 3-mercaptopropyl-trimethoxysilane to a synthesis gel using hydrothermal synthesis techniques [8] that were modified to allow the incorporation and persistence of Au^{3+} cations in the gel at the conditions of synthesis. In a typical synthesis, NaOH (4.8 g) and 3-mercaptopropyl-trimethoxysilane (0.82 g) were added to deionized H_2O (17.9 MΩ resistance; 18 cm^3) in an open 125 cm^3 polypropylene container and stirred by a magnetic bar (6.7 Hz; 8 h); during this process the methanol formed by hydrolysis of the ligands (Section 3.1) evaporates, thus preventing methanol from reducing the Au^{3+} precursors when they are added later. An aqueous solution of $HAuCl_4$·$3H_2O$ (0.26 g) in deionized H_2O (18 cm^3) was added dropwise to the basic methanol-free ligand solution under agitation by a magnetic bar (6.7 Hz) over a period of 0.5 h. Colloidal silica (10.67 g, Ludox AS-30) was added to the polypropylene container, which was capped, sealed, and heated to 353 K under agitation by a magnetic bar (6.7 Hz) for 0.5 h. Finally, $NaAlO_2$ (6.0 g) dissolved in deionized H_2O (18 cm^3) was added dropwise to the Au^{3+}, ligand, and silica solution and mixed by magnetic stirring (6.7 Hz) for 2 h at ambient temperature; this led to a homogeneous synthesis gel with molar ratios of 1.7 SiO_2/1 Al_2O_3/3.2 Na_2O/110 H_2O/0.02 Au/0.12 ligand. The gel was heated at 373 K while magnetically stirring (6.7 Hz) for 12 h under its autogenous pressure to form AuNaLTA. The Au content in the final solids (as measured by optical emission spectroscopy, discussed in Section 2.3) was adjusted by increasing or decreasing the amount of added Au to achieve 0.5–1.0 wt.% theoretical loadings, while keeping a constant 3-mercaptopropyl-trimethoxysilane to Au molar ratio of 6. The solids formed were filtered (Pyrex 3606

fritted funnel, 4–5.5 μm), washed with deionized water until the rinse liquids reached a pH 7–8, and treated in a convection oven at 373 K for 8 h. The solids were heated in flowing dry air (1.67 $cm^3 g^{-1} s^{-1}$) from ambient to 623 K (or 573 K; at 0.033 K s^{-1}) and held for 2 h, cooled to ambient temperature, and then heated to 623 K (or 573 K; at 0.033 K s^{-1}) in flowing H_2 (1.67 $cm^3 g^{-1} s^{-1}$) and held for 2 h.

The air and H_2 treated AuNaLTA zeolites were Ca^{2+} ion exchanged [20] to convert them into AuCaLTA before use in catalytic or characterization studies. AuCaLTA was prepared by adding AuNaLTA (1–5 g) to an aqueous 1 M solution of $CaCl_2 \cdot 2H_2O$ (1 g AuNaLTA per 100 cm^3) and stirring magnetically (6.7 Hz) at ambient temperature for 8 h. The exchange was repeated ten times (to achieve complete exchange, Section 3.4.2) and the solids were filtered and washed with deionized water (1500 $cm^3 g^{-1}$), then treated in stagnant ambient air at 373 K for 12 h.

2.2.2. Au cluster encapsulation within MFI

A hydrothermal MFI synthesis technique [23] which uses TPAOH as a structure-directing agent (SDA) was modified with the addition of Au^{3+} and 3-mercaptopropyl-trimethoxysilane to form AuNaMFI. TPAOH (16.5 g of 1 M solution) and 3-mercaptopropyl-trimethoxysilane (0.28 g) were mixed in a 100 cm^3 polypropylene bottle and stirred magnetically (6.7 Hz) for 8 h in ambient stagnant air. A solution containing $HAuCl_4 \cdot 3H_2O$ (0.088 g) in deionized H_2O (1.88 cm^3) was added dropwise to the ligand/TPAOH solution under agitation by a magnetic bar (6.7 Hz) over a period of 0.5 h, followed by the addition of TEOS (17.3 g). The resulting mixture was sealed with the bottle's cap and further agitated for 13 h at ambient temperature, after which a mixture of TPAOH (13.2 g of 1 M solution), $NaAlO_2$ (0.59 g), and deionized H_2O (1.88 cm^3) was added to it in order to prepare the synthesis gel (6.5 TEOS/2.3 TPAOH/0.56 $NaAlO_2$/120 H_2O/0.035 Au/0.20 ligand molar ratios). The gel was heated to 371 K while magnetically stirring (6.7 Hz) and held for 2 h under its autogenous pressure, then cooled to ambient temperature and transferred to a Teflon-lined stainless steel autoclave (125 cm^3, Parr), in which the gel was held at 393 K for 15 h to form AuNaMFI. The Au content in AuNaMFI was varied by changing the concentrations of the Au precursor and the 3-mercaptopropyl-trimethoxysilane ligand in the synthesis gel (1:6 molar ratio) to obtain 0.2–2.0 wt.% theoretical loadings. AuNaMFI solids were recovered by filtration (Pyrex 3606 fritted funnel, 4–5.5 μm), washed with deionized water to a rinse pH of 7–8, and treated for 8 h at 373 K in ambient air.

Thermal treatments of these AuNaMFI catalysts in dry air and H_2 were varied to establish protocols that form small (~2 nm) and monodisperse Au clusters free of synthetic debris—the characterization of these clusters is discussed in Sections 2.3,3.1 and 3.3. Changes in the Au particle size and surface cleanliness that resulted from incremental increases in treatment temperature and duration, or the application of multiple treatment steps in succession, were evaluated to find the optimal conditions that were then used throughout this study. In the most effective procedure, the AuNaMFI sample was first treated in flowing dry air (1.67 $cm^3 g^{-1} s^{-1}$) and heated from ambient temperature to 546 K (at 0.033 K s^{-1}) and held for 2 h, then cooled to ambient temperature; it was then treated in flowing H_2 (1.67 $cm^3 g^{-1} s^{-1}$) by heating to 546 K (at 0.033 K s^{-1}) and held for 2 h, then allowed to cool to ambient temperature a second time. The sample was further treated in flowing dry air (1.67 $cm^3 g^{-1} s^{-1}$) under a ramped heating procedure in which the temperature was raised to 573 K and held for 2 h, then increased to 648 K and held for 2 h, and finally heated to 723 K and held for 4 h, with a ramp rate of 0.017 K s^{-1} between each step. The Au cluster accessibility and size distribution achieved in AuNaMFI (discussed in Section 3) required the identification and use of these treatment protocols.

2.2.3. Synthesis of silica-supported Au clusters

Au clusters dispersed on SiO_2 (Cab-O-Sil, HS-5, 310 $m^2 g^{-1}$) were prepared using an $Au(en)_2Cl_3$ (en = ethylenediamine) complex previously shown to lead to small clusters [24]. $Au(en)_2Cl_3$ was prepared by dissolving $HAuCl_4 \cdot 3H_2O$ (1.0 g) in deionized H_2O (10 cm^3) and ethylenediamine (0.40 g) was then added. The solution was agitated by magnetic stirring (6.7 Hz) at ambient temperature for 0.5 h, and ethanol (70 cm^3) was then added to cause precipitation; the slurry was stirred for an additional 0.33 h and the solids were recovered by filtration and treated in ambient stagnant air at 313 K for 12 h.

Au/SiO_2 was prepared by dissolving $Au(en)_2Cl_3$ (0.03 g) in deionized H_2O (50 cm^3) and raising the pH to 10 by adding 1.0 M NaOH; SiO_2 (1.0 g) was added to the solution and 1.0 M NaOH was again used to adjust the pH to 10. The suspension was heated to 338 K while stirring for 2 h, filtered and washed with 1500 cm^3 deionized H_2O, and treated in stagnant ambient air at 343 K for 5 h. These Au/SiO_2 samples were heated from ambient to 423 K (at 0.033 K s^{-1}) in flowing H_2 (1.67 $cm^3 g^{-1} s^{-1}$) and held for 2 h. The samples were then cooled to ambient temperature, and finally heated to 673 K (at 0.033 K s^{-1}) in flowing dry air (1.67 $cm^3 g^{-1} s^{-1}$) and held for 2 h. These procedures were previously shown to form active Au clusters free of C and N residues from the ethylenediamine ligands [24]. Brønsted acid sites originating from the silica support can form acid-catalyzed products or secondary alkanol ODH products [25]. A small number of experiments intended to detect the presence of Brønsted acid sites on the silica support (Section 3.4.1) were therefore conducted, before which the Au/SiO_2 catalysts were further treated in 0.05 M NaOH (100 $cm^3 g^{-1}$) at ambient temperature for 2 h with magnetic stir bar agitation (6.7 Hz), and finally recovered by filtration (Pyrex 3606 fritted funnel, 4–5.5 μm) then washed with 500 $cm^3 g^{-1}$ of deionized H_2O.

2.3. Characterization of zeolite structures and embedded Au clusters

Au contents were measured by inductively coupled plasma optical emission spectroscopy (ICP-OES) using a Perkin Elmer 5300 DV optical emission ICP analyzer. X-Ray diffractograms (XRD) were used to determine the phase purity of zeolites and to confirm the absence of large (>10 nm) Au clusters. Diffractograms were measured with a D8 Discover GADDS Powder Diffractometer using Cu Kα radiation ($\lambda = 0.15418$ nm, 40 kV, 40 mA). Samples were mounted on quartz slides by placing and leveling finely-ground powders; diffractograms were measured for 2θ values between 5° and 50° with a scan rate of 0.00625° s^{-1}.

UV–visible spectra were used to monitor the Au localized surface plasmon resonance (LSPR) band during or following treatment of AuNaLTA and Au/SiO_2 in air or H_2. Spectra were acquired using a Varian-Cary 6000i spectrometer and a Harrick scientific diffuse reflectance accessory (DRP-XXX) with a reaction chamber add-on (DRA-2CR); the latter was modified with a fritted stainless steel disk at the sample cup to eliminate temperature gradients and to ensure uniform gas flow through the packed powder samples. A heater held underneath the sample holder and a temperature controller (Watlow Series 982) were used to adjust temperatures, which were measured with a type K thermocouple (Omega) embedded in the sample holder wall. UV–vis spectra were acquired on AuNaLTA and Au/SiO_2 samples (0.1 g; <100 μm aggregates), which were heated to 623 K (at 0.033 K s^{-1}) in flowing dry air (1.67 $cm^3 g^{-1} s^{-1}$) and held for 2 h; they were then cooled to ambient temperature, and treated in flowing H_2 (1.67 $cm^3 g^{-1} s^{-1}$) by heating to 623 K (at 0.067 K s^{-1}) and holding for 2.67 h. Background spectra were used to isolate the effect of Au on the UV–vis spectra and were collected after identical treatment procedures on NaLTA or SiO_2 samples synthesized as AuNaLTA or Au/SiO_2 but without adding Au precursors.

Transmission electron micrographs (TEM) were collected at 120 kV with a Philips/FEI Technai 12 microscope. Samples were prepared by suspending ground powders in acetone and dispersing them onto holey carbon films mounted on 400 mesh copper grids (Ted Pella Inc.). Cluster size distributions were measured using >300 particles for each sample to determine surface-averaged cluster diameters $\langle d_{TEM} \rangle$ [26]:

$$\langle d_{TEM} \rangle = \frac{\sum n_i d_i^3}{\sum n_i d_i^2} \qquad (1)$$

where n_i is the number of clusters with diameter d_i. Metal dispersions (D), defined as the fraction of Au atoms exposed at cluster surfaces, were estimated from $\langle d_{TEM} \rangle$ [26]:

$$D = 6 \frac{v_m/a_m}{\langle d_{TEM} \rangle} \qquad (2)$$

where v_m is the bulk atomic density of Au (16.49×10^{-3} nm^3) and a_m is the area occupied by an Au atom (8.75×10^{-2} nm^2) on a polycrystalline surface [27]. Size distributions were also used to calculate the dispersity index (DI), given by the ratio of the surface-averaged ($\langle d_{TEM} \rangle$) to the number-averaged ($\langle d_n \rangle$) diameter [26]:

$$DI = \frac{\langle d_{TEM} \rangle}{\langle d_n \rangle} = \frac{\left(\frac{\sum n_i d_i^3}{\sum n_i d_i^2} \right)}{\left(\frac{\sum n_i d_i}{\sum n_i} \right)} \qquad (3)$$

The DI value provides a metric for particle size uniformity, with unity denoting perfect monodispersity and values <1.5 typically taken as monodisperse distributions [26,28]. Standard deviations of the mean particle diameters are also computed to provide more commonly recognized metrics of the uniformity of particle size distributions.

Infrared (IR) spectra of CO adsorbed on AuCaLTA, AuNaMFI, and Au/SiO$_2$ wafers (40 mg cm^{-2}) were collected to determine the surface cleanliness of Au clusters. Spectra were measured with a Thermo Nicolet 8700 spectrometer equipped with an in situ flow cell. The wafers were treated in flowing H$_2$/He mixtures (8.4 cm^3 g^{-1} s^{-1} H$_2$, 33.6 cm^3 g^{-1} s^{-1} He) by heating to 573 K (at 0.033 K s^{-1}) and holding for 1 h. After cooling in He flow (42.0 cm^3 g^{-1} s^{-1}) to 263 K, the samples were exposed to flowing CO/He mixtures (42.0 cm^3 g^{-1} s^{-1}; 0.1–1.0 kPa CO). Spectral contributions from CO(g) were subtracted from all reported spectra. Each spectrum was normalized by the number of exposed surface Au atoms, calculated from $\langle d_{TEM} \rangle$ and Au contents.

2.4. Catalytic assessment of reactivity and encapsulation

Oxidative dehydrogenation (ODH) turnover rates of ethanol and isobutanol were measured on powders pelleted and sieved to retain 180–250 μm aggregates and held on a porous quartz frit within a quartz tube (10 mm O.D.). Samples were treated in flowing 20% O$_2$/He (1.67 cm^3 g^{-1} s^{-1}) by heating to 673 K (at 0.033 K s^{-1}) and holding for 1 h, then cooled to 393 K before catalytic measurements. Liquid alkanols (ethanol, isobutanol) and deionized water were evaporated into flowing O$_2$/He streams at 393 K using liquid syringe pumps (Cole Parmer, 60061 Series). He and O$_2$ flow rates were adjusted with mass flow controllers (Porter Instrument) to achieve the desired pressures (4 kPa alkanol, 9 kPa O$_2$, 87.5 kPa He, and 0.5 kPa H$_2$O). H$_2$O forms as an ODH product and can act as a co-catalyst (discussed in Section 3.4.1); thus, it was added to maintain a constant concentration throughout the catalyst bed. Alkanol conversions were kept below 3%, and transfer lines were maintained at 393 K to avoid condensation. Ethanol but

not isobutanol can diffuse through the apertures of AuNaLTA and AuCaLTA; thus, their relative rates provide an assessment of the extent to which Au surfaces reside within the protected environment of LTA voids [8,9] (Section 3.4). Comparison of these rates to those measured on Au/SiO$_2$ confirms that the effects of alkanol size on reactivity reflect the confinement of Au clusters. Both alkanols can enter MFI channels; as a result, the ability of AuNaMFI to protect Au surfaces from titration by large poison molecules was used instead to assess encapsulation.

Ethanol ODH on AuNaLTA and Au/SiO$_2$ was also carried out in the presence and absence of thiophene in the reactant stream (0 vs 0.1 kPa thiophene) to probe the fraction of the Au surfaces protected from contact with thiophene, as a result of their confinement within LTA voids. AuNaMFI, in contrast, was treated ex-situ with dibenzothiophene and then used in ethanol ODH to examine the fraction of the Au surface accessible to DBT. These treatments exposed AuNaMFI and the Au/SiO$_2$ reference (0.1 g) to DBT dissolved in liquid ethanol (30 cm^3; DBT/Au = 6 molar) for 4 h with magnetic stirring (6.7 Hz) at ambient temperature. Samples were then filtered and treated in stagnant dry air at 343 K for 12 h, and used in ethanol ODH reactions at 393 K without further pretreatment (to avoid DBT desorption/decomposition). AuNaMFI and Au/SiO$_2$ control samples were prepared through an analogous procedure without DBT, then used for ethanol ODH. The controls were next heated to 673 K with 0.033 K s^{-1} for 1 h under 20% O$_2$/He (1.67 cm^3 g^{-1} s^{-1}), then cooled back to 393 K for use in ethanol ODH a second time. These controls were used to distinguish the effects of DBT on the measured rate from effects caused by the absence of high temperature pretreatment (673 K O$_2$/He) (Section 3.4.3).

Selectivities are reported on a carbon basis as the fraction of converted alkanol appearing as a particular product. Turnover rates are defined as the molar alkanol conversion rates per surface Au atom (from Au content and $\langle d_{TEM} \rangle$). NaLTA, CaLTA, NaMFI, fumed silica, and empty reactors did not lead to detectable product formation. Measured turnover rates were unaffected by dilution (10:1 mass acid-washed fumed SiO$_2$:Au catalyst) within aggregates or within the packed bed (10:1 mass acid-washed quartz:Au catalyst); thus, measured rates are not corrupted by concentration or temperature effects. Deactivation was not detected over the timescale of these experiments (~5 h), except on Au/SiO$_2$, which exhibited half-lives of 14 and 11 h during ethanol and isobutanol ODH, respectively. Turnover rates on Au/SiO$_2$ were extrapolated to the start of each experiment. Effluent concentrations were measured by gas chromatography (Shimadzu GC-2014) using a methylsilicone capillary column (HP-1; 50 m × 0.32 mm, 1.05 μm film thickness) and a flame ionization detector.

3. Results and discussion

3.1. Zeolite-encapsulated Au nanoparticle synthesis and characterization

X-Ray diffractograms confirmed the presence of the intended zeolite frameworks in AuNaLTA and AuNaMFI samples after treatment in flowing dry air and then H$_2$ (up to 623 K for AuNaLTA, 723 K for AuNaMFI) (Fig. 1). Their crystallinities were 98% and 96% for AuNaLTA (1.1 wt.% Au) and AuNaMFI (1.9 wt.% Au), respectively, as determined from the integrated intensities of the three most intense Bragg lines, using Au-free NaLTA and NaMFI as standards. Diffraction lines for Au metal were not detected in these samples, and their crystallinity was unchanged by thermal treatments as high as 823 K in air or H$_2$. These zeolite materials are crystalline, stable during thermal treatments, and do not contain
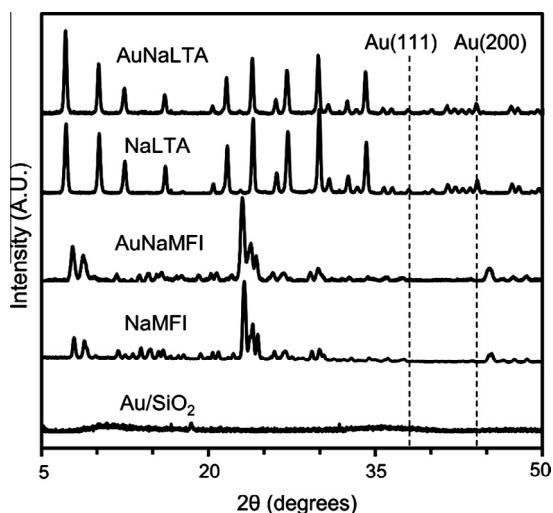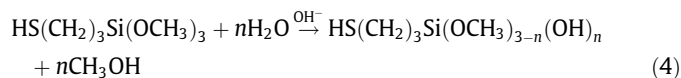
Fig. 1. XRD patterns of AuNaLTA, AuNaMFI, and Au/SiO$_2$ samples.

large Au crystallites (>10 nm), which would have been evident in the diffractograms.

AuNaLTA and AuNaMFI samples were white powders after treatment in ambient air at 373 K and did not exhibit detectable LSPR bands (at 500–600 nm) [29] or ligand-to-metal charge transfer bands (LMCT, 300–500 nm) [30] in their UV–visible spectra. These data show that Au^0 clusters larger than 2 nm are not present [31] and suggest the presence of intact Au–S adducts, which do not exhibit LMCT or LSPR bands [32,33]. Also, Au clusters were not detected by TEM in as-synthesized AuNaLTA or AuNaMFI after treatment at 373 K in ambient air. Thus, we conclude that Au^{3+} centers in the ligated complexes do not reduce to form Au^0 during the hydrothermal synthesis protocols or the crystallization of MFI or LTA frameworks. Such permanence at the pH and temperature of these hydrothermal syntheses indicates that Au^{3+} complexes are effectively stabilized by mercaptosilane ligands. The ethylenediamine ligands in the Au(en)$_2$Cl$_3$ chelate complex, in contrast, reduce Au^{3+} even in inert atmospheres at temperatures as low as 343 K [12], making such ligands unsuitable as stabilizing species during hydrothermal synthesis.

The mercaptosilane ligands form CH$_3$OH molecules in alkaline solution during the displacement of their methoxy groups with hydroxyl groups via hydrolysis:

$$HS(CH_2)_3Si(OCH_3)_3 + nH_2O \xrightarrow{OH^-} HS(CH_2)_3Si(OCH_3)_{3-n}(OH)_n$$
$$+ nCH_3OH \tag{4}$$

The evaporative removal of the CH$_3$OH formed in these reactions is required before hydrothermal synthesis, because CH$_3$OH acts as a reductant for Au^{3+} precursors, even when stabilized by mercaptosilane ligands. Analogous AuNaLTA synthesis protocols using ethylenediamine ligands (to form Au(en)$_2$Cl$_3$) led to large Au^0 crystallites during zeolite crystallization; such species were evident from the marked changes in the color of the synthesis gels (from clear to blue to mauve) as the temperature increased from 300 K to 373 K. These changes, indicative of the formation of Au^0 colloids [7], were confirmed by the presence of large Au clusters (>6 nm) in micrographs of the LTA solids formed via hydrothermal synthesis (Fig. S1, SI).

The presence of Au^{3+} cations uniformly dispersed within LTA or MFI crystals, enforced by the stabilization conferred by mercaptosilane ligands and by the pre-emptive removal of CH$_3$OH reductants, allows their systematic reduction to Au^0 via post-synthetic thermal or chemical treatments, specifically designed to preserve

the encapsulation and monodispersity of small (~1 nm) clusters. Such treatments and their consequences for the size and location of Au clusters were examined by UV–visible spectroscopy and TEM microscopy, as well as by probe reactions that determine the extent to which host zeolites prevent molecules larger than their apertures from accessing active Au surfaces (Section 3.4).

The intensity of the LSPR band in the UV–visible spectra of AuNaLTA (1.1 wt.%) was monitored during heating in flowing dry air and then in flowing H$_2$ (from ambient temperature to 623 K in both cases) to track the formation and growth of Au^0 clusters from the cationic Au precursors (Fig. 2). The LSPR intensity serves as a diagnostic of Au^0 clusters larger than 2 nm, the diameter at which they incipiently exhibit plasmon resonance [31]. These LSPR bands were centered at 506 nm; this wavelength is characteristic of Au^0 clusters smaller than 5 nm, but it is not otherwise sensitive to cluster size [31].

A weak and barely detectable LSPR band emerged during thermal treatments in air between ambient temperature and 623 K, a procedure shown to combust and remove C-atoms from the mercaptosilane ligands (Fig. 2) [8]; these data show that this treatment did not form Au^0 clusters, apparently because strong Au–S bonds prevent Au^{3+} reduction at these conditions. As-synthesized Au/SiO$_2$, consisting of mesoporous SiO$_2$ with deposited Au(en)$_2$Cl$_3$ (Section 2.2.3), in contrast, exhibited an intense plasmon resonance after similar treatments in air (Fig. S2, SI). Such plasmon resonances demonstrate the strong tendency of Au^{3+} to reduce to Au^0, even with protecting ligands and in oxidizing environments, and provide compelling evidence for the greater stability conferred to Au^{3+} by mercaptosilane ligands. Exposing AuNaLTA to pure H$_2$ after air treatment at 623 K led to a sharp increase in the intensity of the LSPR band at 540–623 K (Fig. 2). This increase in intensity reflects the reduction of Au^{3+} by H$_2$ after the oxidative removal of C-atoms from occluded mercaptosilane ligands, which may obstruct H$_2$ from accessing Au^{3+} cations. Treatment of as-synthesized AuNaLTA in pure H$_2$ at 623 K (1.67 cm^3 g^{-1}; 0.067 K s^{-1}) for 2 h without a preceding air treatment at 623 K, however, also led to nearly identical increases in the plasmon band intensity in the same temperature range (540–623 K; Fig. S3, SI). These data show that the protecting ligands do not obstruct H$_2$ access to Au^{3+} cations and that the H$_2$ treatment is solely responsible for decomposing Au–S adducts and for forming Au^0 species, which subsequently migrate throughout the zeolite crystal to form metal clusters. Au plasmon resonance bands are also evident in AuNaLTA after only treatment in air at 723 K (1.67 cm^3 g^{-1}; 0.067 K s^{-1}) for 2 h (Fig. S4, SI), indicating that Au–S adducts decompose and form Au^0 (even without H$_2$ treatment) at sufficiently high temperatures. Air treatment alone can reduce Au^{3+} cations, but the use of H$_2$ allows reduction at lower temperatures, an important requirement to preserve Au dispersion, monodispersity, and encapsulation during the critical reduction process.

The strong effects of H$_2$ treatment temperature (540–623 K) on the intensity of LSPR bands (Fig. 2), and on the Au^0 cluster size that such features reflect, were examined to determine whether the mean particle diameter in AuNaLTA could be systematically varied through changes in the H$_2$ treatment temperature protocols. AuNaLTA was first treated in air (to remove C residues) and then in H$_2$ at several temperatures within the critical range for Au^{3+} reduction (540–623 K) evident from UV–vis spectra (Fig. 2), and the resulting Au particle size distributions were measured using TEM micrographs. Post-synthetic treatment of AuNaLTA (1.1 wt.%) in flowing air at 573 K (or 623 K) and then in pure H$_2$ at 573 K (or 623 K) (each for 2 h) gives Au clusters with surface-averaged diameters of 1.3 nm (or 2.3 nm) (Fig. 3, Table 1). These clusters were nearly monodisperse in both cases (1.07 and 1.09 DI), indicating that cluster growth occurred without detectable loss of uniformity.
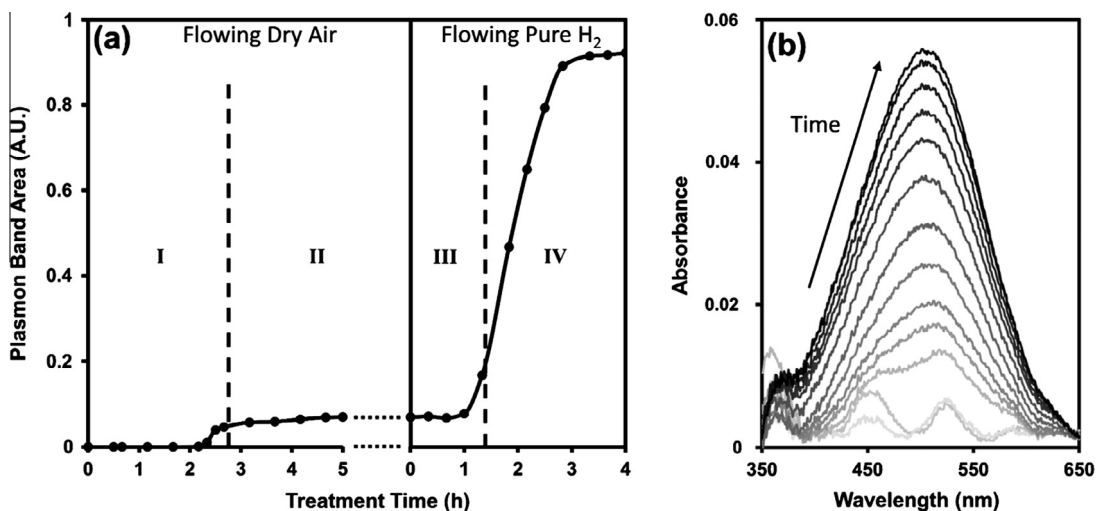
Fig. 2. (a) Evolution of the 1.1 wt.% AuNaLTA LSPR band integrated intensity in flowing air (I and II) or H_2 (III and IV) under (I): 120 K h^{-1} ramp to 623 K, (II): 623 K, (III): 240 K h^{-1} ramp to 623 K, subsequent to cooling to ambient temperature after (II), and (IV): 623 K. (b) Growth of the LSPR band for 1.1 wt.% AuNaLTA (following 2 h treatment at 623 K under air flow) in flowing H_2 over the temperature range 543–623 K (240 K h^{-1} ramp to 623 K, 0.17 h between each spectrum) corresponding to hours 1–3 in regions (III) and (IV) in (a). Gas flows were operated at 1.67 cm^3 g^{-1} s^{-1} and 100 kPa with dry air or pure H_2.
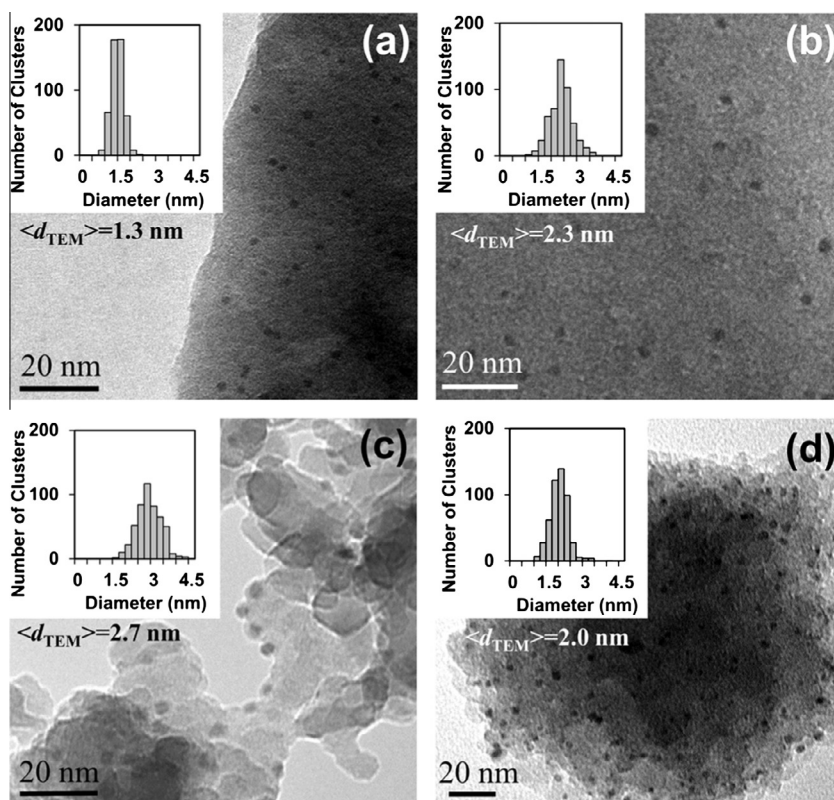

Fig. 3. TEM micrographs, surface-averaged Au cluster diameters, $\langle d_{TEM} \rangle$ (Eq. (1)), and cluster diameter distributions for (a) 1.1 wt.% AuNaLTA post-synthetically treated at 573 K, (b) 1.1 wt.% AuNaLTA post-synthetically treated at 623 K, (c) 2.2 wt.% Au/SiO$_2$, and (d) 1.9 wt.% AuNaMFI.

We surmise that such size uniformity reflects the condensation of silanols with the protecting ligands attached to Au^{3+} cations to form siloxane bridges within the synthesis gel or within the structural building units involved in the nucleation and growth of the zeolite framework. Such chemical linkages would favor the uniform incorporation of Au^{3+} precursors throughout the zeolite crystals [8] and the ultimate orderly migration of Au^0 species as such precursors reduce to form clusters uniform in size and dispersed throughout the zeolite void space. The smaller clusters evident at

lower treatment temperatures in H_2 may reflect the less mobile nature of incipiently-reduced Au precursors, denuded of some mercaptosilane ligands, at these temperatures, thus favoring the formation of a larger number of nucleation points and, consequently, of smaller Au^0 clusters. The small Au clusters (1.3 nm) formed by H_2 treatment at 573 K are similar or slightly larger than the NaLTA α-cages (1.1 nm) [8], and occupy approximately 1.5% of these α-cages for the 1.1 wt.% Au loading sample (calculations in SI; Section 5, Eq. (S1)) [9]. The 2.3 nm clusters formed by H_2

Table 1

Metal Loadings, surface averaged particle diameters, and normalized CO–Au IR intensities of Au-zeolite catalysts synthesized with the hydrothermal technique, and a reference Au/SiO_2 sample.

Sample	Metal loading (wt.%)[a]	Au cluster diameter $\langle d_{TEM}\rangle$ (nm)[b]	D[c]	DI[d]	Ω[e]
AuNaLTA	1.1	1.3 ± 0.2	0.89	1.07	0.9 ± 0.1
AuNaLTA	1.1	2.3 ± 0.4	0.51	1.09	1.1 ± 0.1
AuNaLTA	0.5	2.2 ± 0.4	0.53	1.08	1.1 ± 0.1
AuNaMFI	0.2	2.1 ± 0.4	0.55	1.06	0.9 ± 0.1
AuNaMFI	1.9	2.0 ± 0.4	0.58	1.09	1.2 ± 0.1
Au/SiO_2	2.2	2.7 ± 0.5	0.43	1.06	–

[a] Analyzed by inductively coupled plasma optical emission spectroscopy.
[b] Surface area weighted mean cluster diameter determined via TEM (Eq. (1)).
[c] Dispersion estimated from $\langle d_{TEM}\rangle$ (Eq. (2)).
[d] Dispersity Index computed as the surface averaged cluster diameter divided by the number averaged diameter (Eq. (3)).
[e] Ratio of sample's integrated CO–Au IR band intensity to that of Au/SiO_2 under 1 kPa CO and 99 kPa He at 263 K, where intensities for each are normalized by the number of surface Au atoms in the sample (as estimated by the metal loading and D) (Eq. (5)). NaLTA samples were cation exchanged with Ca^{2+} before IR measurements to improve the accessibility of CO to the zeolite interior.

treatment at 623 K occupy approximately 0.26% of these α-cages. These clusters exceed the size of the LTA α-cages, indicating that they locally disrupt the LTA framework, but the small number and extent of such disruptions preclude their detection in diffractograms [9]. In spite of these local disruptions, such Au clusters are protected by the large number of intervening windows and cages among clusters and between the clusters and the external crystal surfaces, thereby conferring stability against coalescence, as well as reactant shape selectivity in catalytic reactions (Section 3.4.2). The mean size, but not the dispersity of these clusters, is sensitive to the temperature at which their cationic precursors are reduced; thus, their dispersion can be systematically controlled through variations in the H_2 treatment temperature.

The precise control of Au cluster size is more challenging for MFI than LTA frameworks, because organic SDA species (TPAOH) occluded within the zeolite must be removed to allow access to intracrystalline voids and to any active surfaces therein. Air treatments for 2–3 h above 720 K completely combust and remove TPAOH [34]. Treating as-synthesized AuNaMFI (1.9 wt.%) in flowing dry air (1.67 $cm^3\,g^{-1}\,s^{-1}$) from ambient temperature to 723 K (0.033 $K\,s^{-1}$) and holding for 3 h, however, led to the formation of relatively large Au particles (3.2 nm; 1.12 DI; Fig. S5, SI). A similar treatment with a slower temperature ramp (0.016 $K\,s^{-1}$) formed slightly smaller clusters (3.0 nm; 1.09 DI; Fig. S6, SI). It seems plausible that oxidation of intracrystalline SDA moieties causes local exotherms, thus precluding precise local temperature control as Au^0 forms and favoring cluster growth. Such effects were minimized using a stepped temperature ramping protocol (Section 2.2.2) to 723 K in air, intended to decrease SDA oxidation rates and allow heat dissipation; this strategy led to much smaller (2.0 nm) and nearly monodisperse (1.09 DI) Au clusters (TEM; Fig. 3, Table 1). As in the case of Au clusters in LTA, these clusters are larger than the largest voids in MFI (channel intersections; 0.64 nm) [21]; yet, they are thermally stable (Section 3.2), reside within the zeolite crystals (Section 3.4.3), and are protected against sintering and access by large molecules by many intervening channels among clusters and between the clusters and the external zeolite surfaces.

The size and dispersity of Au clusters in AuNaMFI and AuNaLTA prepared using these treatment protocols were essentially unaffected by Au loading (0.5–1.1 wt.% in LTA; 0.2–1.9 wt.% in MFI; Table 1). Syntheses with higher Au loading (⩾6 wt.%) led to amorphous materials (Fig. S7, SI) apparently because of competition for the intracrystalline void space within incipiently formed nuclei between the SDA species (Na^+ for LTA or TPAOH for MFI), needed

to template the crystalline voids, and the mercaptosilane ligands needed to protect and disperse the Au^{3+}. AuNaLTA treated in air at 623 K then H_2 at 623 K gave clusters with 2.3 nm surface-averaged diameter and DI values of 1.08 and 1.09 for 0.5 wt.% and 1.1 wt.% Au contents, respectively. Similarly, AuNaMFI with 0.2 wt.% and 1.9 wt.% Au gave clusters with diameters of 2.1 nm (1.06 DI) and 2.0 nm (1.09 DI), respectively. Au clusters occupy <0.5% of the intracrystalline void volume in these LTA and MFI samples [9,21], and TEM micrographs (Fig. 3) suggest that the Au clusters are uniformly dispersed throughout LTA and MFI crystals.

We therefore conclude that the uniform dispersion of the ligand-stabilized precursors throughout the synthesis gel, and ultimately throughout the zeolite crystals, leads to large and uniform spacing among precursors and to limited cluster growth processes. The driving force for such cluster growth, reflecting the tendency of small particles to minimize their surface energy, tends to weaken in magnitude as the cluster size increases and is likely resisted sterically by the surrounding framework. Such resistance probably includes the kinetic hurdles imposed by large numbers and small sizes of the intervening apertures and the thermodynamic barriers imposed by the energy required to locally disrupt the zeolite framework to accommodate larger clusters. We surmise that the clusters continue to grow until the driving force for their expansion is balanced by these barriers against further disruption of the framework.

3.2. Thermal stability of Au clusters in LTA and MFI

The stability of Au^0 clusters in AuNaLTA (1.1 wt.%) and AuNaMFI (1.9 wt.%) (prepared as described in Sections 2.2.1 and 2.2.2, respectively) was then examined during treatment in flowing dry air by heating to a final temperature between 623 and 873 K at 0.033 $K\,s^{-1}$ and holding for 5 h. Their surface-averaged cluster diameters and DI values, derived from TEM micrographs, are shown in Fig. 4 as a function of this final temperature. The cluster diameters were unchanged by treatment temperatures below 773 K (1.3 nm NaLTA; 2.0 nm NaMFI); their size and dispersity increased slightly between 773 K and 823 K and then significantly at temperatures above 823 K (2.1 nm AuNaLTA; 2.6 nm AuNaMFI). Similar treatment protocols using pure H_2 instead of air at 773 K did not cause detectable cluster growth in AuNaMFI or AuNaLTA, but some slight growth was detected after treatments between 773 K and 823 K and became more evident above 823 K (1.9 nm AuNaLTA; 2.5 nm AuNaMFI) (Table S1, SI). The treatment atmosphere (air or pure H_2) did not have any detectable effects on the stability of the Au clusters, apparently because Au surfaces remain essentially bare above 600 K in both environments [35], thus preventing adsorbed species from altering surface energies or atomic mobility, which influence, in turn, coalescence and Ostwald ripening. The stability of Au clusters in AuCaLTA, the Ca^{2+} exchanged form of AuNaLTA (Section 2.2.1), was also examined using analogous air or H_2 treatments at 773 K. The Ca^{2+} exchange was performed to enlarge the apertures in NaLTA [20] before using it in CO adsorption (Section 3.3; Section S9, SI) or catalytic reaction studies (Section 3.4.1), so as to improve the access of diffusing molecules to Au cluster surfaces. The Au cluster size (1.3 nm) and dispersity index (1.07) in AuCaLTA also did not change following these air or H_2 treatments, indicating that the ion exchange process did not adversely affect Au cluster size or stability.

The size, stability, and dispersity of these Au clusters within AuNaLTA, AuCaLTA, and AuNaMFI represent significant improvements over those reported for clusters dispersed on mesoporous supports. Deposition-precipitation or impregnation of Au onto TiO_2 gives Au^0 particles as small as 3.2 nm [36], but treatment in 8% O_2/He for 2 h at 773 K causes extensive cluster agglomeration to form particles >10 nm in diameter [6]. Deposition-
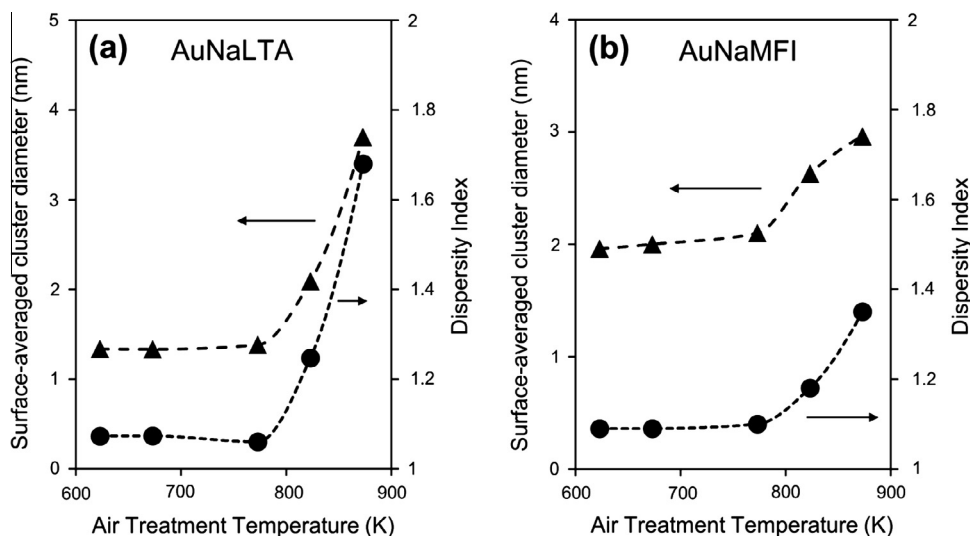
Fig. 4. Effect of flowing dry air treatment temperature (21 kPa O_2, 79 kPa N_2, 1.67 cm^3 g^{-1} s^{-1}, 5 h) on the TEM-derived surface averaged cluster diameter ($\langle d_{TEM} \rangle$, ▲) (Eq. (1)), and dispersity index (DI, ●) (Eq. (3)) of Au clusters in (a) 1.1 wt.% AuNaLTA and (b) 1.9 wt.% AuNaMFI.

precipitation techniques on γ-Al_2O_3 supports form slightly larger 3.5 nm particles, which grow to 4.0 nm after treatment for 2 h at 873 K in 25% O_2/He [13]. Au clusters deposited onto mesoporous silicas (SBA-11, SBA-12, SBA-15, HMM-2, and MCM-41) functionalized with amines sinter to form 4.3–7.9 nm particles after treatment in pure H_2 at 473 K for 2 h [37]. Metal sputter deposition techniques, although difficult to implement at practical scales [38,39], form Au clusters that are among the smallest and most stable [6]. For example, sputtering Au metal onto fumed SiO_2 gives particles with 2.5 nm mean diameter (but also several large (>10 nm) clusters), which grow to 3.2 nm after annealing at 773 K in 8% O_2/He for 2 h [6]. AuNaLTA (1.3 nm) and AuNaMFI (2.0 nm), by contrast, maintain smaller and nearly monodisperse clusters after similar treatments. The size stability conferred to Au clusters by encapsulation appears to reflect their uniform dispersion throughout crystals and their inhibited migration and coalescence caused by the small apertures connecting LTA and MFI voids. The Au metal clusters within these voids do not coalesce up to 773 K, temperatures well above those used during the post-synthetic H_2 reduction (573–623 K) that forms them, showing that desirable dispersions can be maintained at higher temperatures after Au metal clusters form, as long as the critical Au^{3+} reduction step is systematically controlled.

3.3. Assessment of exposed Au surfaces by chemisorbed CO

Infrared absorption bands of CO adsorbed on AuCaLTA, AuNaMFI, and Au/SiO_2 were examined to assess the cleanliness and accessibility of their Au metal surfaces. This technique was used instead of chemisorptive titrations that are challenging or infeasible for Au^0 particles in zeolites. The chemisorption of H_2 and O_2 onto Au^0, for instance, is slow and seldom equilibrated at temperatures required for significant coverages because of high dissociation activation barriers [35]. The molecular adsorption of CO occurs on both Au clusters and zeolite counterions [40] and cannot be distinguished from volumetric uptakes.

The IR spectra of CO adsorbed on the Au clusters in AuNaMFI (1.9 wt.%; $\langle d_{TEM} \rangle$ = 2.0 nm), AuCaLTA (1.1 wt.%; $\langle d_{TEM} \rangle$ = 2.3 nm), and Au/SiO_2 (2.2 wt.%; $\langle d_{TEM} \rangle$ = 2.7 nm) at 263 K under 1 kPa CO are shown in Fig. 5a. Spectral intensities are normalized by the number of surface Au atoms.

AuNaMFI and Au/SiO_2 samples exhibit absorption bands at 2108 cm^{-1} and 2109 cm^{-1} respectively, which correspond to atop

adsorption of CO on Au^0 [41]. AuCaLTA showed two separate bands, both at higher frequencies than those for CO–Au^0 in AuNaMFI and Au/SiO_2. The more intense band at 2177 cm^{-1} corresponds to CO adsorbed onto charge-balancing Ca^{2+} cations in LTA [40,42]. The second band at 2123 cm^{-1} corresponds to CO on Au sites in AuCaLTA. The contributions to this spectrum from Ca^{2+}–CO species were subtracted using the CO infrared bands on CaLTA (Fig. S8, SI) to obtain accurate intensities and frequencies for the Au–CO bands. The Au–CO band in AuCaLTA is shifted to higher frequencies (by 14 cm^{-1}) relative to that for CO–Au^0 in Au/SiO_2. This shift likely reflects slightly electron-deficient Au surfaces ($Au^{\delta+}$) [41,43,44], which decrease back-donation from Au to $2\pi^*$ orbitals in adsorbed CO, thus increasing the C–O bond force constant and increasing its vibrational frequency [43]. Such effects have been reported for Pt, Pd, and Au clusters within FAU, and reflect electron withdrawal from metal centers by the electropositive charge-balancing zeolite cations [43,45,46]. We consider this to add circumstantial evidence indicating that the Au clusters are located within LTA voids, where the Ca^{2+} cations must reside. The absence of similar shifts (relative to Au/SiO_2) on AuNaMFI reflects the higher valence of Ca^{2+} (in LTA) relative to Na^+ (in MFI), and also the higher density of cations in LTA (0.24 Ca^{2+}/T atom, where T = Si, Al; Si/Al = 1.1 vs. 0.03 Na^+/T atom; Si/Al = 31).

In what follows, we measure the effects of CO pressure on Au–CO band intensities for AuCaLTA, AuNaMFI, and Au/SiO_2 to determine the number and relative binding strength of CO binding sites. In doing so, we compare the number of exposed Au atoms in these materials to determine whether the Au clusters evident in their TEM micrographs exhibit clean surfaces available for CO chemisorption.

The integrated intensities of the Au–CO bands in AuCaLTA, AuNaMFI, and Au/SiO_2 are shown in Fig. 5b (263 K, 0.1–1.0 kPa CO). These normalized intensities (by saturation values at 1.0 kPa) reflect the CO fractional coverage at accessible Au surface atoms, but not the absolute amounts of chemisorbed CO. The Au–CO bands in all samples shift to slightly lower frequencies as pressure increases from 0.1 to 1.0 kPa CO (~4.2 cm^{-1}; Fig. S9, SI), a result of weakening Au–CO interactions as CO coverage increases [47]. Increases in the Au–CO band intensities with pressure are significantly weaker at the high end of the pressure range (~7% increase from 0.8 to 1.0 kPa) than the low end (~21% increase from 0.1 to 0.2 kPa) for all samples, suggesting that coverages are near to saturation values at 1.0 kPa. CO fractional coverages are similar on
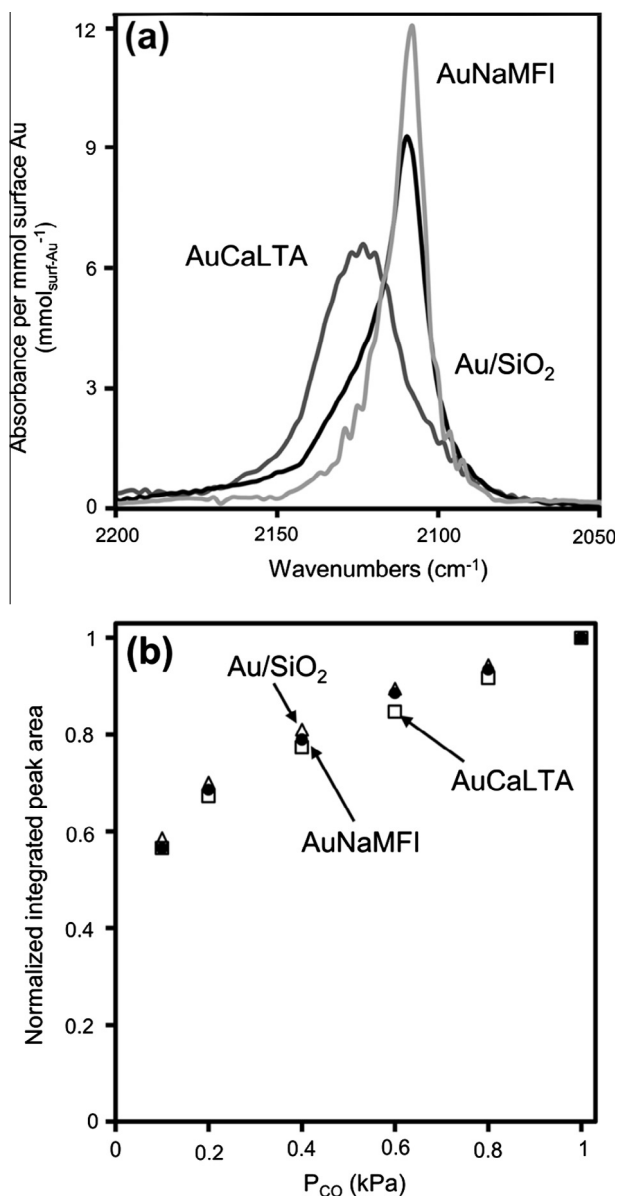
Fig. 5. (a) Infrared spectra of CO adsorbed on Au clusters in Au/SiO₂ (black), AuCaLTA (gray), and AuNaMFI (light gray) samples at 263 K (1.0 kPa CO, 99.0 kPa He) after flowing H₂ pretreatment (573 K, 20 kPa H₂, 80 kPa He). Spectral intensities are normalized by the moles of exposed surface Au in each sample (estimated with dispersions derived from TEM micrographs and metal loadings measured with ICP-OES analysis). (b) Integrated peak areas for AuCaLTA (□), AuNaMFI (●), and Au/SiO₂ (△) measured at 263 K over the range 0.1–1 kPa CO, where areas are normalized by the maximum collected area (at 1 kPa CO) for each respective sample.

chiometries and infrared absorption cross-sections are also similar, thus allowing absolute comparisons of band intensities to determine the number of surface atoms that are able to bind CO for each sample. These comparisons of the CO binding provide a measure of the surface cleanliness of samples prepared by mercaptosilane-stabilized precursors.

The surface cleanliness of Au clusters in AuCaLTA and AuNaMFI is quantified by a factor Ω_i:

$$\Omega_i = \frac{\tilde{I}_i}{\tilde{I}_{Au/SiO_2}} \qquad (5)$$

where $\tilde{I}_i$ is the integrated Au–CO band intensity for catalyst i (i = AuCaLTA, AuNaMFI, Au/SiO₂) normalized by the number of surface Au atoms in the sample. $\tilde{I}_{Au/SiO_2}$ is used as the reference because the oxidative treatments (673 K, 2 h, Section 2.2.3) we apply to Au/SiO₂ are known to remove all synthetic debris from the sample, as shown conclusively by temperature programmed oxidation experiments and thermal gravimetric analysis [24]. Consequently, Ω_i values near unity reflect similarly clean and accessible Au surfaces in AuCaLTA or AuNaMFI. The Ω_i values were computed using normalized CO IR spectra collected at 1 kPa and are shown in Table 1. Errors in these values are estimated as ±10% based on the standard deviation of three unique measurements of $\Omega_{AuCaLTA}$ (for 1.1 wt.% AuCaLTA; $\langle d_{TEM}\rangle$ = 2.3 nm), computed using three measurements of $\tilde{I}_{Au/SiO_2}$ and $\tilde{I}_{AuCaLTA}$. All Ω_i values are close to unity (0.9–1.2), confirming the cleanliness and accessibility of the Au clusters in AuCaLTA and AuNaMFI. These Ω_i values indicate that the air and H₂ treatments applied to the Au-zeolite catalysts (to 673 K in air; 573 K in H₂) are effective at removing S species, derived from mercaptosilane ligands, from Au cluster surfaces. Indeed, mercaptosilane ligands can be removed from Au⁰ clusters at even lower temperatures (573 K, 1 h, air flow) [49] and even from Pt, Pd, and Ir clusters (623 K, 2 h flowing H₂ treatment) [8] in spite of stronger S binding on these metals than on Au (Pt–S: 233 kJ mol⁻¹; Pd–S: 183 kJ mol⁻¹; Ir–S: 206 kJ mol⁻¹; Au–S: 126 kJ mol⁻¹) [50,51]. The data shown in this section provide compelling evidence that the post-synthesis treatments used here lead to accessible and clean Au clusters.

3.4. Consequences of encapsulation for catalysis and the use of turnover rates and large titrants to determine encapsulation selectivities

Our evidence for the presence of Au clusters within zeolite voids in AuNaLTA, AuCaLTA, and AuNaMFI based on their size (Section 3.1), stability (Section 3.2), and CO binding properties (Section 3.3) seems compelling. They are small in size (1.3–2.0 nm), similar to the dimensions of zeolite voids (1.1 nm LTA; 0.64 nm MFI), and seem uniformly dispersed throughout zeolite crystals (TEM; Fig. 3). They are exceptionally resistant to sintering by comparison with Au clusters dispersed on mesoporous supports, a property that we infer must reflect their restricted mobility through confinement and the thermodynamic hurdles imposed by the need to disrupt LTA and MFI frameworks to grow. The Au$^{\delta+}$-CO IR bands in AuCaLTA suggest a proximity between Au clusters and Ca²⁺ counterions that can only be reconciled with confinement. Yet, their catalytic properties remain the ultimate arbiter of surface cleanliness and the raison d'etre for the effort spent in their synthesis. Reactivity, in the form of turnover rates, depends sensitively on the amount and cleanliness of the exposed Au surfaces; the selective preference for reactions of smaller molecules and a resistance to poisoning by large titrants, in turn, would provide the quantitative measures of encapsulation.

these samples in spite of the slightly electron-deficient cluster surfaces in AuCaLTA, indicating that the higher CO vibrational frequencies (relative to Au⁰) do not lead to detectable effects on CO binding energies. Density functional theory calculations of chemisorbed CO on Pt(1 1 1) surfaces with a mathematically imposed slight positive charge show a 20 cm⁻¹ increase in frequency, but a small decrease in CO binding energy (<5 kJ mol⁻¹) at 0.25 fractional coverages, which becomes even smaller as coverages increase [48]. Physical mechanisms and magnitudes of such shifts in frequencies and binding energies are expected to be similar for other metals, including Au [48]. The similar CO fractional coverages on AuCaLTA, AuNaMFI, and Au/SiO₂ suggest that CO interacts similarly with their respective surfaces, indicating that binding stoi-

3.4.1. Alkanol oxidative dehydrogenation (ODH) on Au-zeolite catalysts

Zeolites bring forth remarkable diversity into the catalytic chemistries of encapsulated metal clusters through their ability to select reactants, products, and transition states based on their molecular size and shape [8,9]. Here, we exploit such zeolite shape selectivity effects by measuring ODH turnover rates of ethanol (0.40 nm kinetic diameter) [9] and isobutanol (0.55 nm kinetic diameter) [9] on AuNaLTA (0.42 nm aperture) [9] and AuCaLTA (0.50 nm aperture) [20] to quantify the extent to which active Au surfaces reside within zeolite voids. The windows in NaLTA and CaLTA allow ethanol diffusion into the void space but essentially exclude isobutanol; thus, comparison of ODH turnover rates for small and large alkanols on unrestricted surfaces (e.g. Au/SiO₂) and on AuCaLTA or AuNaLTA allows rigorous estimates of the fraction of the exposed metal atoms that reside within the LTA void space.

The slow diffusion of reactants in small-pore zeolites, such as LTA, can be enhanced by replacing the resident cations with ions that have smaller atomic radii or higher valence [52]. Ca^{2+} exchange into NaLTA decreases the total number of counterions in the framework and leads to larger effective window apertures that increase diffusion rates [52]; therefore, ODH rates on AuNaLTA and AuCaLTA can be used to determine the extent to which intracrystalline concentration gradients of alkanol reactants affect measured rates. NaMFI channels (0.55 nm apertures) cannot exclude isobutanol from intracrystalline voids. Consequently, the relative rates of ethanol and isobutanol ODH cannot be used to determine the extent of encapsulation in AuNaMFI. Instead, encapsulation is probed by determining the fraction of Au cluster surfaces that are protected from titration by a poison (dibenzothiophene; DBT, 0.9 nm kinetic diameter) that cannot enter MFI crystals (Section 3.4.3).

Alkanol ODH reactions form water and alkanals as primary products [25,53]. These alkanals can undergo oxidation to carboxylic acids, which, in turn, can react with alkanols in esterification reactions [53] on Brønsted acids to form hemiacetals that dehydrogenate oxidatively on Au to form esters [54]. These Brønsted acid sites can also catalyze elimination reactions of alkanols to form ethers and alkenes [25,53]. H_2O, formed as an ODH co-product, increases the rate of kinetically-relevant O_2 activation steps in ODH reactions via the formation of peroxide or hydroperoxide species, thus acting as an ODH co-catalyst [55]. In doing so, H_2O circumvents difficult O_2 dissociation steps, which exhibit high activation barriers on Au surfaces [13], and removes the requirement for coordinatively unsaturated Au atoms prevalent on small clusters [55], making even large Au clusters remarkably active in alkanol oxidations [55,56]. These effects of H_2O make reactivity comparisons among catalysts difficult because axial H_2O gradients lead to non-uniform reactivity along the catalyst bed, even at low alkanol conversions. These effects are eliminated here by adding H_2O to the reactant stream at concentrations 5-10 times larger than those imposed by ODH reactions and by operating at low alkanol conversions (<3.0%), which also minimize secondary reactions.

Secondary ODH products (esters, carboxylic acids, ethers) were not detected on any Au-zeolite catalysts, but Au/SiO₂ formed ethyl acetate from ethanol (10.0% selectivity at 2.4% conversion) and isobutyl-isobutyrate from isobutanol (8.7% selectivity at 2.1% conversion). These secondary reactions do not affect measured turnover rates, because the formation of each product requires one initial ODH event, in which an alkanal forms via kinetically-relevant β-H abstraction from an adsorbed alkoxide by chemisorbed oxygen atoms [57]. Exposure of Au/SiO₂ to 0.05 M NaOH (as described in Section 2.2.3) to titrate H^+ species by Na^+ led to much lower ethyl acetate selectivities (4.8% vs. 10.0%) without

detectably influencing ODH turnover rates. These data show that esters form on Au/SiO₂ because of the presence of Brønsted acid sites.

3.4.2. ODH catalytic evidence for cluster encapsulation within LTA

The selectivity of Au encapsulation in AuNaLTA and AuCaLTA can be measured from the ratio of ODH turnover rates for ethanol ($r_{ethanol}$) and isobutanol ($r_{isobutanol}$) reactants, defined as

$$\chi_{ODH,i} = \frac{r_{ethanol}}{r_{isobutanol}} \qquad (6)$$

where i represents a given sample (AuNaLTA, AuCaLTA, AuNaMFI). These χ_{ODH} values are expected to be larger on AuNaLTA and AuCaLTA than those on AuNaMFI or Au/SiO₂, because the former two samples but not the latter two prevent access to intracrystalline Au clusters by isobutanol reactants. The χ_{ODH} value for Au/SiO₂ ($\chi_{ODH,Au/SiO_2}$) reflects the relative intrinsic reactivities of ethanol and isobutanol in the absence of diffusional constraints for either alkanol, because SiO₂ mesopores do not selectively exclude the larger alkanol. The ratio of these χ_{ODH} values for each Au-zeolite sample to that of Au/SiO₂ defines an encapsulation selectivity parameter ϕ:

$$\phi = \frac{\chi_{ODH,i}}{\chi_{ODH,Au/SiO_2}} \qquad (7)$$

which determines, in turn, the extent to which active Au surface atoms reside within microporous voids that ethanol, but not isobutanol, can access. ϕ values approach unity for Au clusters that are freely accessible to both alkanols, such as those dispersed in MFI or mesoporous SiO₂. Large ϕ values, by contrast, suggest that Au clusters are predominantly secluded from contact by isobutanol. Clusters encapsulated within LTA should be completely inactive in isobutanol ODH, because LTA apertures are small enough to fully exclude isobutanol from its void structure. As a result, ϕ values for AuNaLTA and AuCaLTA represent the ratio of the total active Au surface area in the sample to that of fully accessible Au clusters at external zeolite crystal surfaces. The selectivity parameters then give the fraction of the Au surface area contained within voids (F) as follows:

$$F = 1 - \frac{1}{\phi} \qquad (8)$$

Large ϕ values (e.g. $\phi > 10$, which implies $F > 0.90$; Eq. (8)) thus provide evidence that Au clusters predominantly reside within zeolite voids, and are taken here as evidence of successful encapsulation.

Table 2 shows ethanol and isobutanol ODH turnover rates, χ_{ODH} values, and the resulting encapsulation selectivity parameters for Au/SiO₂ and Au-zeolite catalysts. The ratios of ethanol to isobutanol ODH rates on AuNaLTA and AuCaLTA (33–133) are much larger than on AuNaMFI (1.8) or Au/SiO₂ (1.5), consistent with Au clusters predominantly residing within LTA crystals, which in contrast with Au clusters in MFI or SiO₂ structures, are prevented from contact with isobutanol. The resulting encapsulation selectivities (ϕ, Eq. (7)) are large (22–57). These ϕ values correspond to >95% ($F > 0.95$; Eq. (8)) of the Au surface area in AuNaLTA and AuCaLTA residing within the protected microporous voids of LTA crystals.

Ethanol ODH turnover rates varied somewhat among LTA-based Au catalysts with changes in Au content and cluster size, and as Na^+ was replaced with Ca^{2+} via post-synthesis exchange. AuCaLTA (2.3 nm clusters; 1.1 wt.% Au; 0.017 s⁻¹) gave larger ODH turnover rates than AuNaLTA (2.3 nm; 1.1 wt.%; 0.004 s⁻¹) (Table 2), apparently because slight ethanol concentration gradients were weakened as diffusivities increased when Ca^{2+} replaced Na^+ cations. Ethanol ODH turnover rates increased monotonically as Ca^{2+} ions

Table 2
Catalytic properties of Au-encapsulated LTA, MFI, and Au/SiO$_2$ catalysts in oxidative dehydrogenation (ODH) of alkanols.[a]

Sample	Au cluster diameter $\langle d_{TEM} \rangle$ (nm)	Metal loading (wt.%)	Alcohol ODH turnover rate (10^{-3} s^{-1} mol$^{-1}_{surf-Au}$)			
			$r_{ethanol}$[b]	$r_{isobutanol}$[b]	χ_{ODH}[c]	ϕ[d]
AuCaLTA	1.3 ± 0.2	1.1	12	0.14	86	57
AuCaLTA	2.3 ± 0.4	1.1	17	0.15	113	76
AuCaLTA	2.2 ± 0.4	0.5	22	0.20	110	73
AuNaLTA	2.3 ± 0.4	1.1	4	0.12	33	22
AuNaMFI	2.0 ± 0.4	1.9	16	9	1.8	1.2
Au/SiO$_2$	2.7 ± 0.5	2.2	33	22	1.5	–

[a] Oxidative Dehydrogenation: 4 kPa alkanol, 9 kPa O$_2$, 0.5 kPa H$_2$O, balance He to 101 kPa at 393 K.
[b] Reaction turnover rate defined as number of moles of reactant converted per time normalized by the number of exposed surface metal atoms estimated by TEM.
[c] $\chi_{ODH} = r_{ethanol}/r_{isobutanol}$ (Eq. (6)).
[d] Ratio of the χ_{ODH} value for the sample to that of Au/SiO$_2$ (Eq. (7)).

replaced two Na$^+$ ions with each additional exchange cycle (Section 2.2.1) (Fig. S10, SI) and then reached constant values after ten exchange cycles. The Ca/Al ratio (measured by ICP) after ten exchange cycles was 0.47, similar to the value expected from complete exchange (0.50). These monotonic changes continue up to the point of full exchange, suggesting that Ca^{2+} weakens, but does not remove, ethanol concentration gradients that lead to turnover rates lower than their kinetic limit.

The AuCaLTA sample with larger Au particles (1.1 wt.%; 2.3 nm) gave slightly higher ethanol ODH turnover rates (0.017 s^{-1}; Table 2) than that with smaller Au clusters (1.1 wt.% 1.3 nm; 0.012 s^{-1}), an unexpected finding in view of ethanol ODH turnover rates that depend only weakly on Au cluster size [58]. These trends do not reflect residues derived from protecting ligands, because the intensity of their respective CO infrared bands are proportional to their TEM-derived cluster dispersions (see Ω_i values; Eq. (5); Table 1; Section 3.3). Their different rates reflect instead ethanol concentration gradients that become steeper as the number of Au surface atoms, and therefore the kinetic load, increase with increasing dispersion. Indeed, ethanol turnover rates on AuCaLTA samples (0.022 s^{-1}, 0.017 s^{-1}, 0.012 s^{-1}; Table 2) decrease monotonically as the volumetric density of Au surface atoms increases (0.015, 0.033, 0.057; units (1000 Å^3)$^{-1}$; Eq. (S2), SI); these trends are consistent with intrazeolite ethanol concentration gradients that cause measured rates to be lower than those expected from the (higher) extrazeolite concentrations. The monotonic increase in turnover rates with the number of Ca^{2+} exchange cycles (Fig. S10, SI) further confirms that these ethanol gradients persist even in fully exchanged samples. In contrast with encapsulated Au clusters, Au surfaces in extrazeolitic regions or in mesoporous solids are exposed to the prevalent concentrations of ethanol in the fluid phase, thus operating at the higher alkanol turnover rates characteristic of their kinetic limit. The lower ODH turnover rates on intracrystalline clusters lead, in turn, to ϕ values (Eq. (7)) that underestimate the extent to which Au surfaces reside within the

confining voids in LTA samples. The reported encapsulation selectivity parameters (Table 2) must therefore be considered conservative lower limits of their true values.

3.4.3. Evidence of metal cluster encapsulation in MFI

The encapsulation selectivity of Au clusters in AuNaMFI was determined from measurements of ethanol ODH turnover rates on Au/SiO$_2$ and AuNaMFI samples with and without preceding exposure to dibenzothiophene (DBT) dissolved in ethanol (Section 2.4). Organosulfur compounds, such as thiophene and DBT, irreversibly adsorb onto Au surfaces, both as molecular species and after C–S hydrogenolysis, to form unreactive species that block active surfaces [59]. As a result, ODH turnover rates on Au/SiO$_2$ and on extrazeolite Au clusters in AuNaMFI should be strongly suppressed by DBT, while Au surfaces within intracrystalline MFI regions, which are inaccessible to DBT, should preserve their ODH reactivity in the presence of DBT, thus providing a reliable account of the extent to which Au cluster surfaces lie within the intracrystalline space.

In these experiments, untreated and DBT-treated samples were exposed to air at mild conditions (343 K, Section 2.4) before use in ethanol ODH to remove adsorbed ethanol but to avoid desorbing DBT or its hydrogenolysis products from Au surfaces; such mild treatments may allow samples to retain other residues from the ethanol solvent used to dissolve DBT (Section 2.4). These effects led to only small changes in ODH rates (Table 3), but were taken into account by comparing ODH turnover rates on samples exposed to liquid ethanol with and without dissolved DBT (the latter denoted below as the "control sample") and otherwise identically treated in air at 343 K before catalysis. Turnover rates measured on control samples (AuNaMFI: 0.0094 s^{-1}; Au/SiO$_2$: 0.012 s^{-1}) (Table 3) were slightly lower than those on samples pretreated at higher temperature (673 K; AuNaMFI: 0.016 s^{-1}; Au/SiO$_2$: 0.033 s^{-1}). Treatment of the control samples at this higher temperature leads to full recovery in the ODH rates (Table 3), consistent with the desorption of contaminants that could not be removed by the milder air treatment.

ODH turnover rates measured on the control samples (r_{ODH}) and on those exposed to DBT ($r_{ODH,DBT}$) are used to define a parameter Λ_{DBT}:

$$\Lambda_{DBT,i} = \frac{r_{ODH,DBT}}{r_{ODH}} \qquad (9)$$

where i identifies the specific sample (e.g., Au/SiO$_2$, AuNaMFI). A fraction of the Au surfaces exposed to DBT will retain some detectable ODH reactivity, because the binding and surface reactivity of DBT-derived species decreases as surfaces reach near-saturation coverages [60]. As a result, $\Lambda_{DBT,Au/SiO_2}$ reflects the fraction of the Au surface in Au/SiO$_2$ that remains vacant after DBT exposure. $\Lambda_{DBT,AuNaMFI}$ similarly represents the fraction of the Au surfaces that remain active in ODH for AuNaMFI, which would include those

Table 3
Rates of ethanol oxidative dehydrogenation on Au/SiO$_2$ and AuNaMFI following DBT exposure or pretreatment.

Pretreatment	Au-zeolite catalyst ethanol ODH turnover rate (10^{-3} s^{-1} mol$^{-1}_{surf-Au}$)				
	(1) EtOH[a]	(2) EtOH + DBT[b]	(3) 673 K O$_2$[c]	(4) EtOH → 673 K O$_2$[d]	Λ_{DBT}[e]
AuNaMFI	9.4	8.9	16	16	0.95
Au/SiO$_2$	12	1.3	33	34	0.11

[a] Samples (100 mg) agitated in 30 cm^3 of EtOH at ambient temperature for 4 h, treated in ambient air at 343 K for 12 h, then used in ODH reaction (393 K under 9 kPa O$_2$, 4 kPa EtOH, and 0.5 kPa H$_2$O).
[b] Samples treated analogously with (1), but with dissolved DBT in the EtOH at a 6:1 DBT:Au molar ratio.
[c] Fresh samples treated in flowing 20% O$_2$/He (1.67 cm^3 g^{-1} s^{-1}, 2 h), then used in reaction.
[d] Sample (1) was treated in flowing 20% O$_2$/He (1.67 cm^3 g^{-1} s^{-1}, 2 h) and used again in a second reaction.
[e] Ratio of rates from samples (2) and (1) (Eq. (9)).

cluster surfaces confined within MFI crystals. These ratios are used to define an encapsulation selectivity parameter (ϕ_{DBT}) as follows:

$$\phi_{DBT} = \frac{\Lambda_{DBT,AuNaMFI}}{\Lambda_{DBT,Au/SiO_2}} \qquad (10)$$

As in the case of similar parameters for LTA samples (Eq. (7); Section 3.4.2), a ϕ_{DBT} value of unity would reflect Au clusters that are fully accessible to DBT in MFI samples, thus indicating their exclusive presence at extracrystalline regions. Values of ϕ_{DBT} much larger than unity are taken as a measure of successful encapsulation procedures. ϕ_{DBT} values, similar to the values of ϕ (Eq. (7)), give the ratio of the total Au surface area to that present at extrazeolite Au clusters, thus allowing the determination of the fraction of the Au surface area that is encapsulated (F)

$$F = 1 - \frac{1}{\phi_{DBT}} \qquad (11)$$

The ethanol ODH turnover rates and their associated $\Lambda_{DBT,i}$ values for AuNaMFI (1.9 wt.%; $\langle d_{TEM} \rangle$ = 2.0 nm) and Au/SiO$_2$ (1.1 wt.%; $\langle d_{TEM} \rangle$ = 2.7 nm), as well as the treatment conditions for these catalysts, are shown in Table 3. The ODH turnover rates on AuNaMFI exposed to DBT (0.0089 s^{-1}) and on the DBT-free control sample (0.0094 s^{-1}) were similar, thus resulting in a $\Lambda_{DBT,AuNaMFI}$ value near unity (0.95). The turnover rate on the DBT-treated Au/SiO$_2$ sample (0.0013 s^{-1}), in contrast, was about ten times smaller than that on the DBT-free Au/SiO$_2$ control (0.012 s^{-1}), resulting in a small $\Lambda_{DBT,Au/SiO_2}$ value (0.11) (Eq. (9)). These data lead in turn to an encapsulation selectivity parameter of 8.6 (ϕ_{DBT}, Eq. (10)) for AuNaMFI, and to the conclusion that ~90% of its Au surface area resides within the protected voids of MFI crystals (Eq. (11)).

Ethanol ODH turnover rates on samples treated at 673 K were slightly lower for AuNaMFI (0.016 s^{-1}; Table 3) than Au/SiO$_2$ (0.033 s^{-1}); this difference does not reflect Au surface contamination derived from mercaptosilane ligand residues, because the surface-normalized CO IR bands for these samples (Ω_i; Eq. (5); Table 1) are of equal intensity. We attribute these different rates instead to diffusional constraints for ethanol within MFI crystals. Such constraints may result from relatively slow rates of intracrystalline diffusion, or from pore blockage at the crystallite outer surface by a layer of silicates [61–64], which may be formed as by-products during MFI crystallization through the action of the organic templates [64].

3.5. Protection of LTA-encapsulated Au clusters from thiophene poisoning

The selective encapsulation of Au clusters within LTA, evident from the relative rates of ethanol and isobutanol ODH (Section 3.4.2), should also protect such clusters from thiophene, which, as in the case of isobutanol, cannot diffuse within LTA voids. This is shown here from ethanol ODH rates on AuNaLTA and Au/SiO$_2$ in the presence or absence of thiophene. NaLTA is used, because its apertures (0.42 nm) are smaller than those of CaLTA (0.50 nm) and thus more effectively exclude thiophene poisons (0.46 nm kinetic diameter) [9]. These data are used to confirm the high encapsulation selectivities determined from ethanol and isobutanol ODH turnover rates.

Ethanol ODH rates (divided by their initial value) are shown in Fig. 6 as a function of time for AuNaLTA and Au/SiO$_2$ with 0 kPa and 0.1 kPa of thiophene in the reactor feed. ODH rates on AuNaLTA gradually decreased to 80% of their initial value after 2 h of exposure to thiophene, without detectable changes upon thiophene removal from the inlet stream. On Au/SiO$_2$, rates decreased to 6% of their initial value over 2 h of exposure, then recovered slightly (to 11%) upon thiophene removal, likely because some thiophene
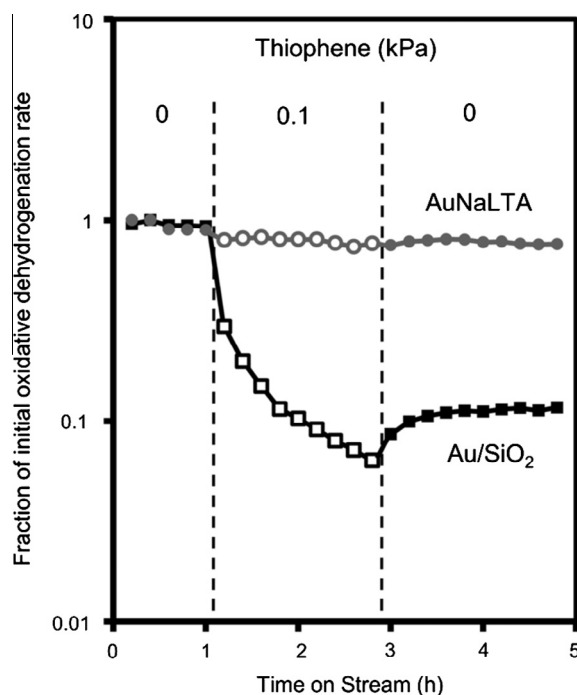

Fig. 6. Ratio of the initial ethanol oxidative dehydrogenation rate at 393 K under 9 kPa O$_2$, 4 kPa EtOH, and 0.5 kPa H$_2$O (rates quantified in terms of s^{-1} mol$_{surf-Au}^{-1}$) to those exhibited in the presence (0.1 kPa, open markers) and absence (closed markers) of thiophene under continuous reaction for AuNaLTA (●) and Au/SiO$_2$ (■).

desorbed from Au clusters [65], an effect that was not evident in AuNaLTA apparently because of the relatively small fraction of the Au surface in unprotected extracrystalline regions.

These data can be used to confirm the encapsulation selectivities reported in Section 3.4.2 from ethanol and isobutanol ODH rates, using a formalism similar to that developed for AuNaMFI using DBT poisons (Section 3.4.3). Ethanol turnover rates on AuNaLTA and Au/SiO$_2$ before (r_{ODH}) and after ($r_{ODH,TP}$) thiophene poisoning for 2.0 h are defined as follows:

$$\Lambda_{TP,i} = \frac{r_{ODH,TP}}{r_{ODH}} \qquad (12)$$

where i represents a given sample (Au/SiO$_2$, AuNaLTA). This $\Lambda_{TP,i}$ parameter accounts for the fraction of the Au surfaces that are inaccessible to thiophene in each sample. Similar to ϕ_{DBT} (Eq. (10)), an encapsulation selectivity parameter (ϕ_{TP}) is defined as

$$\phi_{TP} = \frac{\Lambda_{TP,AuNaLTA}}{\Lambda_{TP,Au/SiO_2}} \qquad (13)$$

which gives the ratio of the total Au surface area in AuNaLTA to that residing in unprotected extrazeolite environments. As in the case of ϕ (Eq. (7)), this selectivity parameter underestimates the true extent of encapsulation, because intracrystalline ethanol concentration gradients cause ODH rates on encapsulated Au clusters to be smaller than those on Au surfaces at fully accessible locations. The measured $\Lambda_{TP,AuNaLTA}$ and $\Lambda_{TP,Au/SiO_2}$ values were 0.77 and 0.063 respectively, giving a ϕ_{TP} value of 12.8 and an F value of 0.92, consistent with the conclusions reached from the relative turnover rates of ethanol and isobutanol ODH on these samples ($F > 0.95$, Section 3.4.2).

These data, taken together, provide compelling evidence for the selective encapsulation of Au clusters within zeolites. Encapsulation was achieved in both LTA and MFI, zeolites with significantly different aperture sizes (8-MR, 0.42 nm; 10-MR, 0.55 nm), Si/Al ratios (1.1; 31), void environments (supercages; channel

intersections), synthesis templates (Na⁺, inorganic SDA; TPAOH, organic SDA), and silica sources (colloidal SiO_2; TEOS). In spite of this diversity in framework structure, composition, and required synthesis reagents, Au precursors were confined within zeolites and subsequent thermal treatments led to their reduction and the nucleation of nearly monodisperse clusters ~1–2 nm in size and with clean surfaces using the same mercaptosilane ligands and synthesis protocols. These ligands disperse Au^{3+} precursors throughout zeolite crystals as they incipiently form and prevent their premature reduction and agglomeration at the pH and temperatures required for crystallization of the microporous frameworks. The small and monodisperse nature of these clusters reflects the uniform dispersion and the restricted mobility of their ligand-stabilized precursors, imposed by the small interconnecting channels in the microporous networks and the systematic control of the rates of reduction and of ligand removal from these precursors. Such protocols and mechanistic insights can be translated broadly into successful general strategies for the encapsulation of Au clusters within diverse frameworks, within which, as shown in this study, they can be protected structurally and chemically and used to catalyze reactions only of those reactant molecules that can access their surfaces via diffusion through their intracrystalline voids.

4. Conclusion

A broadly applicable procedure was developed for the encapsulation of small (1–2 nm) and nearly monodisperse Au clusters within zeolites using a ligand-assisted hydrothermal synthesis protocol. The encapsulation of Au particles in LTA and MFI zeolites are demonstrated as specific examples of the proposed technique. The synthetic procedure employs mercaptosilane ligands, which bind to and chemically protect Au^{3+} cations against reduction as they are introduced into zeolite synthesis gels. These ligands simultaneously form siloxane bridges with silicate precursors to promote the uniform incorporation of Au into the zeolite host. Treatment of the crystallized zeolites in O_2 and then H_2 reduces the Au^{3+} cations, which form dispersed and encapsulated clusters. The mean size of these clusters can be systematically adjusted, without losses in monodispersity, through simple modifications in the reduction temperature. The Au particles remain sinter-stable to 773 K in air or H_2 as a result of their confinement in zeolite voids, which restrict their mobility and the size to which they can grow. The encapsulated clusters also show high size selectivity during catalytic oxidative alkanol dehydrogenation or exposure to organosulfur poisons, because they are secluded from contact by molecules larger than the zeolite apertures. The encapsulated Au surfaces were free of synthetic debris and accessible to CO, as determined by the analysis of adsorbed CO IR bands. The present work outlines the synthesis of Au clusters whose average size can be controlled while maintaining stability and a narrow size distribution, allowing the systematic study of Au clusters at reaction conditions which strongly favor Au particle sintering into large, inactive agglomerates. We predict that the proposed strategy will have wide applicability for the encapsulation of Au into zeolites with different framework topologies, compositions, and void environments. The proposed method extends the currently available Au encapsulation techniques to include small-pore (⩽8 MR) zeolites, for which the use of cation-exchange or impregnation techniques is not feasible.

Notes

The authors declare the following competing financial interest(s): (1) The funding for the research came from Chevron Energy Technology Co. and (2) Stacey I. Zones is an employee of this company and, more generally, is also a stockholder in Chevron Corp.

Appendix A. Supplementary material

TEM micrographs and particle size distribution of Au clusters in AuNaLTA synthesized with $Au(en)_2Cl_3$; UV–Vis spectra of Au/SiO_2 and AuNaLTA treated in air; trends in plasmon band intensities of AuNaLTA during treatment in H_2 only; the formula for the fraction of occupied α-cages in AuNaLTA; TEM micrographs and particle size distributions for AuNaMFI samples; diffractograms for >6 wt.% AuNaLTA and AuNaMFI samples; mean particle sizes in AuNaLTA and AuNaMFI after treatments in H_2; IR spectra of CO on CaLTA, AuCaLTA, and Au/SiO_2; ethanol ODH rates on partially Ca^{2+} exchanged AuNaLTA samples; the formula to calculate the volumetric density of Au surface atoms in AuCaLTA. Supplementary data associated with this article can be found, in the online version, at http://dx.doi.org/10.1016/j.jcat.2016.04.015.

References

[1] A. Abad, A. Corma, H. García, Chem. Eur. J. 14 (2008) 212–222.
[2] T. Mallat, A. Baiker, Chem. Rev. 104 (2004) 3037–3058.
[3] G.J. Hutchings, Chem. Commun. (2008) 1148–1164.
[4] M. Shekhar, J. Wang, W.-S. Lee, W.D. Williams, S.M. Kim, E.A. Stach, J.T. Miller, W.N. Delgass, F.H. Ribeiro, J. Am. Chem. Soc. 134 (2012) 4700–4708.
[5] J. Mielby, J.O. Abildstrøm, F. Wang, T. Kasama, C. Weidenthaler, S. Kegæs, Angew. Chem. Int. Ed. 53 (2014) 12513–12516.
[6] G.M. Veith, A.R. Lupini, S.J. Pennycook, D.R. Mullins, V. Schwartz, C.A. Bridges, N.J. Dudney, J. Catal. 262 (2009) 92–101.
[7] G. Schmid, B. Corain, Eur. J. Inorg. Chem. 2003 (2003) 3081–3098.
[8] M. Choi, Z. Wu, E. Iglesia, J. Am. Chem. Soc. 132 (2010) 9129–9137.
[9] Z. Wu, S. Goel, M. Choi, E. Iglesia, J. Catal. 311 (2014) 458–468.
[10] P.B. Weisz, V.J. Frilette, R.W. Maatman, E.B. Mower, J. Catal. 1 (1962) 307–312.
[11] D. Guillemot, M. Polisset-Thfoin, J. Fraissard, Catal. Lett. 41 (1996) 143–148.
[12] S. Zeng, S. Ding, S. Li, R. Wang, Z. Zhang, Inorg. Chem. Commun. 47 (2014) 63–66.
[13] M. Ojeda, B.-Z. Zhan, E. Iglesia, J. Catal. 285 (2012) 92–102.
[14] A.B. Laursen, K.T. Højholt, L.F. Lundegaard, S.B. Simonsen, S. Helveg, F. Schueth, M. Paul, J.D. Grunwaldt, S. Kegæs, C.H. Christensen, K. Egeblad, Angew. Chem. Int. Ed. 49 (2010) 1026–1033.
[15] K.T. Højholt, S.K. Laursen, C.H. Christensen, Top. Catal. 54 (2011) 1026–1033.
[16] J. Gu, Z. Zhang, P. Hu, L. Ding, N. Xue, L. Peng, X. Guo, M. Lin, W. Ding, ACS Catal. 5 (2015) 6893–6901.
[17] R. Celis, M. Carmenhermosiän, J. Cornejo, Environ. Sci. Technol. 34 (2000) 4593.
[18] S.J.L. Billinge, E.J. McKimmy, S. Shatnawi, H.J. Kim, V. Petkov, D. Wermeille, T.J. Pinnavaia, J. Am. Chem. Soc. 127 (2005) 8492.
[19] M. Choi, H.S. Cho, R. Srivastava, C. Venkatesan, D.-H. Choi, R. Ryoo, Nat. Mater. 5 (2006) 718.
[20] J. Weitkamp, S. Ernst, L. Puppe, in: J. Weitkamp, L. Puppe (Eds.), Catalysis and Zeolites: Fundamentals and Applications, Springer-Verlag, New York, 1999, pp. 354–355.
[21] C. Baerlocher, L.B. McCusker, Database of Zeolite Structures, <http://www.iza-structure.org/databases/>.
[22] B. Van de Voorde, M. Hezinova, J. Lannoeye, A. Vandekerkhove, B. Marszalek, B. Gil, I. Beurroies, P. Nachtigall, D. De Vos, Phys. Chem. Chem. Phys. 17 (2015) 10759–10766.
[23] B. Gevert, L. Eriksson, A. Törncrona, J. Porous Mater. 18 (2011) 723–728.
[24] H. Zhu, Z. Ma, J.C. Clark, Z. Pan, S.H. Overbury, S. Dai, Appl. Catal., A 326 (2007) 89–99.
[25] O.A. Simakova, V.I. Sobolev, K.Y. Koltunov, B. Campo, A.-R. Leino, K. Kordas, D.Y. Murzin, Chem. Cat. Chem. 2 (2010) 1535–1538.
[26] G. Bergeret, P. Gallezot, in: G. Ertl, H. Knozinger, F. Schuth, J. Weitkamp (Eds.), Handbook of Heterogeneous Catalysis, Wiley-VHC, Weinheim, Germany, 2008, pp. 738–765.

[27] W. Luo, M. Sankar, A.M. Beale, Q. He, C.J. Kiely, P.C.A. Bruijnincx, B.M. Weckhuysen, Nat. Commun. 6 (2014) 1–10.
[28] M. Schneider, D.G. Duff, T. Mallat, M. Wildberger, A. Baiker, J. Catal. 147 (1994) 500–514.
[29] S. Kunz, E. Iglesia, J. Phys. Chem. C 118 (2014) 7468–7479.
[30] D.H. Brown, G.C. McKinlay, W.E. Smith, Inorg. Chim. Acta. 32 (1979) 117–121.
[31] S. Peng, J.M. McMahon, G.C. Schatz, S.K. Gray, Y. Sun, Proc. Natl. Acad. Sci. USA 107 (2010) 14530–14534.
[32] Y. Mikhlin, M. Likhatski, A. Karacharov, V. Zaikovski, A. Krylov, Phys. Chem. Chem. Phys. 11 (2009) 5445–5454.
[33] A. Tlahuice-Flores, R.L. Whetten, M. Jose-Yacaman, J. Phys. Chem. C 117 (2013) 12191–12198.
[34] X. Lin, J.L. Falconer, R.D. Noble, Chem. Mater. 10 (1998) 3716–3723.
[35] A.A.C. Carabineiro, B.E. Nieuwenhuys, Gold Bull. 42 (2009) 288–301.
[36] L. Delannoy, N.E. Hassan, A. Musi, N.N.L. To, J.-M. Krafft, C. Louis, J. Phys. Chem. B 110 (2006) 22471–22478.
[37] M.T. Bore, H.N. Pham, E.E. Switzer, T.L. Ward, A. Fukuoka, A.K. Datye, J. Phys. Chem. B 109 (2005) 2873–2880.
[38] C. Terashima, Y. Iwai, S.-P. Cho, T. Ueno, N. Zettsu, N. Saito, O. Takai, Int. J. Electrochem. Sci. 8 (2013) 5407–5420.
[39] A.S. Edelstein, R.C. Cammarata, Nanomaterials: Synthesis, Properties and Applications, IOP Publishing, London, 1996.
[40] C.L. Angell, P.C. Schaffer, J. Phys. Chem. 70 (1966) 1413–1417.
[41] T. Venkov, K. Fajerwerg, L. Delannoy, H. Klimev, K. Hadjiivanov, C. Louis, Appl. Catal., A 301 (2006) 106–114.
[42] V. Rakić, V. Dondur, R. Hercigonja, J. Serb. Chem. Soc. 68 (2003) 409–416.
[43] D. Guillemot, V.Y. Borovkov, V.B. Kazansky, M. Polisset-Thfoin, J. Fraissard, J. Chem. Soc., Faraday Trans. 93 (1997) 3587–3591.
[44] R. Carrasquillo-Flores, I. Ro, M.D. Kumbhalkar, S. Burt, C.A. Carrero, A.C. Alba-Rubio, J.T. Miller, I. Hermans, G.W. Huber, J.A. Dumesic, J. Am. Chem. Soc. 137 (2015) 10317–10325.
[45] W.M.H. Sachtler, Z. Zhang, Adv. Catal. 39 (1993) 129–220.
[46] Z. Karpinski, Adv. Catal. 37 (1990) 45–100.
[47] H. Hartshorn, C.J. Pursell, B.D. Chandler, J. Phys. Chem. C 113 (2009) 10718–10725.
[48] P. Deshlahra, E.E. Wolf, W.F. Schneider, J. Phys. Chem. A 113 (2009) 4125–4133.
[49] N. Zheng, G.D. Stucky, J. Am. Chem. Soc. 128 (2006) 14278–14280.
[50] H. Toulhoat, P. Raybaud, S. Kasztelan, G. Kresse, J. Hafner, Catal. Today 50 (1999) 629–636.
[51] R.G. Nuzzo, F.A. Fusco, D.L. Allara, J. Am. Chem. Soc. 109 (1987) 2358–2368.
[52] D. Bobdok, E. Besedová, Pet. Coal 45 (2003) 19–24.
[53] M.C. Holz, K. Tölle, M. Muhler, Catal. Sci. Technol. 4 (2014) 3495–3504.
[54] T. Mallat, A. Baiker, Annu. Rev. Chem. Biomol. Eng. 3 (2012) 11–28.
[55] C.-R. Chang, X.-F. Yang, B. Long, J. Li, ACS Catal. 3 (2013) 1693–1699.
[56] R.J. Angelici, Catal. Sci. Technol. 3 (2013) 279–296.
[57] B. Xu, R.J. Madix, C.M. Friend, Acc. Chem. Res. 47 (2014) 761–772.
[58] Y. Guan, E.J.M. Hensen, Appl. Catal., A 361 (2009) 49–56.
[59] E.O. Sako, H. Kondoh, I. Nakai, A. Nambu, T. Nakamura, T. Ohta, Chem. Phys. Lett. 413 (2005) 267–271.
[60] R. Meyer, C. Lemire, S.K. Shaikhutdinov, H.J. Freund, Gold Bull. 37 (2004) 72–124.
[61] P. Kortunov, S. Vasenkov, C. Chmelik, J. Kärger, D.M. Ruthven, J. Wloch, Chem. Mater. 16 (2004) 3552–3558.
[62] Y. Fujikata, T. Masuda, H. Ikeda, K. Hashimoto, Micropor. Mesopor. Mater. 21 (1998) 679–686.
[63] A.R. Teixeira, X. Qi, C.-C. Chang, W. Fan, W.C. Conner, P.J. Dauenhauer, J. Phys. Chem. C 118 (2014) 22166–22180.
[64] L. Karwacki, M.H.F. Kox, D.A. Matthijs de Winter, M.R. Drury, J.D. Meeldijk, E. Stavitski, W. Schmidt, M. Mertens, P. Cubillas, N. John, A. Chan, N. Kahn, S.R. Bare, M. Anderson, J. Kornatowski, B.M. Weckhuysen, Nat. Mater. 8 (2009) 959–965.
[65] E. Ito, J. Noh, M. Hara, Jpn. J. Appl. Phys. 42 (2003) L852–L855.